AN EXPERIMENTAL STUDY OF THE EFFECTS OF AQUEOUS POLYMER SOLUTIONS ON A LIQUID BOUNDARY LAYER

BY

CHI-HUNG SHEN, B.Sc. (ENG.) (HON.)

A Thesis

Submitted To The Faculty of Graduate Studies

in Partial Fulfilment of the Requirements

for the Degree

Master of Engineering

McMaster University

May 1968

MASTER OF ENGINEERING (1968) McMASTER UNIVERSITY
(Mechanical Engineering) (Hamilton, Ontario)

TITLE: "An Experimental Study of the Effects of Aqueous Polymer Solutions on a Liquid Boundary Layer"

AUTHOR: Chi-Hung Shen, B.Sc. (Eng.) (Hon.)
(University of Hong Kong)

SUPERVISOR: Dr. B. Latto

NUMBER OF PAGES: vii , 65

SCOPE AND CONTENTS:

This thesis is an experimental study of the effects of injecting dilute polymer solutions into a turbulent boundary layer developed on a flat plate submerged in water.

A flat plate having a plexiglass surface together with a separate leading edge piece were specially designed for observing the boundary layer phenomena. Aqueous polymer solutions were introduced into the boundary layer through a slit situated in the leading edge piece. Hot-film anemometer technique was employed in the measurements of velocity profiles, turbulence intensities and lateral correlation coefficients at several locations on the plate. The investigation was carried out for two Reynolds Numbers, based on the length of the plate, of 2.4×10^5 and 6.4×10^5. The variation in the drag force with respect to the polymer concentrations and the injection rates was assessed based on the velocity profile data. It was found that the

momentum diffusivity was smaller than for pure water, and that the presence of the polymer molecules seemed to promote a more uniform distribution of the sizes of the turbulence eddies.

ACKNOWLEDGEMENTS

The author wishes to express his sincere gratitude to his supervisor, Dr. B. Latto, for the continuous encouragement and assistance given by him throughout the course of the work.

Thanks are also extended to Dr. D. G. Huber and Dr. A. E. Hamielec, from whom much valuable advice and information has frequently been sought.

The technical help in building the equipments from Mr. R. Brown and Mr. J. Crookes is here gratefully acknowledged.

The author wishes to thank Stein-Hall Limited of Westhill, Ontario, which had supplied free of charge the polymer samples used in the experiment.

The research was supported financially by the Defense Research Board of Canada, under Grant Number 9550-25.

CONTENTS

NOMENCLATURE

SYMBOL	DESCRIPTION	UNIT
A	Constant in the hot-film probe calibration equation	$Volt^2/(ft./sec)^n$
A_1	Numerical constant in the universal logarithmic law for turbulent velocity profiles	
B	Numerical constant in the universal logarithmic law for turbulent velocity profiles	
b	Constant in the power law model of a Non-Newtonian fluid	$lbf\ sec^s/ft^2$
c_f	Local skin friction coefficient $= \frac{\tau_o}{\frac{1}{2}\rho U_\infty^2}$	
D	Drag force	lbf
d	Diameter of a circular pipe	ft.
E	d.c. anemometer outfit voltage	volt
E_o	Anemometer voltage at zero velocity	volt
f	Longitudinal velocity correlation coefficient	
g	Lateral velocity correlation coefficient	
k	Prandtl's mixing length constant	
L_f	Longitudinal integral scale $= \int_0^\infty f\,dr$	ft
L_g	Lateral integral scale $= \int_0^\infty g\,dr$	ft

l	Turbulent mixing length	ft
n	Index in the probe calibration equation	
P_{11}, P_{22}, P_{33}	Components of the deviatoric normal stress	lbf/ft^2
Re_x	Reynolds Number $= x U_\infty/\nu$	
r	Distance between two probes in correlation coefficient measurement. Radial coordinate in a pipe.	ft
s	Index in the power law model	
T	Fluid temperature	°F
U	Velocity at any point	ft/sec.
V_{app}	Apparent velocity	ft/sec.
U_∞	Main stream velocity	ft./sec.
u'	R.M.S. value of the longitudinal fluctuating velocity	ft./sec.
U_*	Friction velocity $= \sqrt{\tau_o/\rho}$	ft./sec.
$U+$	Non-dimensional velocity $= U/U_*$	
V	Injection velocity of the polymer solution	ft/sec.
v'	R.M.S. value of the lateral fluctuating velocity, normal to the plate surface	ft/sec.
w'	R.M.S. value of the lateral fluctuating velocity, parallel to the plate surface	ft/sec.
x	Distance along the plate from the leading edge	ft.
y	Distance normal to the plate surface	ft.
$y+$	Non-dimensional distance $= y U_*/\nu$	
δ	Boundary layer thickness	ft.

θ	Momentum thickness	ft.
ν	Kinematic viscosity of fluid	$ft^2/sec.$
η	Velocity ratio = U/U_∞	
β	Normal distance from the plate surface of the fixed probe in correlation coefficient measurement	
ε	Eddy viscosity	$ft^2/sec.$
τ_o	Wall shear stress	lbf/ft^2
τ	Shear stress	lbf/ft^2
ρ	Density of fluid	lb/ft^3
λ_g	Micro-scale of the lateral correlation coefficient	ft.

SUBSCRIPT:

a	For polymer solution

I INTRODUCTION

In recent years the development and applications of synthetic organic polymers have expanded considerably and there is a definite need to understand the fluid mechanics of dilute polymer solutions, especially their drag reduction ability. The drastic decrease in friction resistance in ship model tests has been suggested by many laboratories to be caused by traces of polymers in the towing tanks. Even though the exact working mechanism is still under investigation, low concentration polymer additives are presently being used to reduce the drag in the pumping of oils, water and other liquids over long distances. By adding minute quantities of the polymers to the main solution, say for example, a few p.p.m.*, the required pumping power is reduced considerably.

Furthermore, the concentration of the polymers present are so low that the solutions for all practical purposes retain their original physical properties. They are thus, in essence, still Newtonian fluids in character but contain some long coiled chains of molecules to alter some other obscure, undefined fluid properties. Up to the present, there appears to be no rigorous satisfactory explanation for this flow phenomenon exhibited by the very dilute polymer solutions.

---

* p.p.m. parts of solute in one million parts of solvent, by weight.

It has been conjectured that the visco-elastic properties of the polymer solutions play an important role in the drag reduction effects but still the determining parameters have not yet been identified.

This thesis is an experimental study on the turbulent boundary layer over a flat plate situated in a water channel. Aqueous polymer solutions of polyacrylamides+ in various concentrations were injected through a slit, situated at the leading edge of the plate, into the main stream. It has been observed by Smallman(1)++ of this laboratory, who used a rotating disc apparatus, that a drag reduction of up to 50% could be achieved from this particular polymer solution. The work reported here attempted to determine its influences on the velocity profiles, turbulence scales and the shear stress on the plate surface. The thesis serves as a preliminary investigation for future research on boundary layer controls and turbulence suppression in this laboratory.

+ MRL-295 Processed by Stein Hall Ltd., No.-average mol. wt. about 3×10^6.

++ Numbers in brackets designate references

II LITERATURE SURVEY

II.1 Experiments and Theories on Drag Reduction:

For a comprehensive review on the investigations and theoretical analysis on the drag reduction by polymer solutions, it is suggested that reference be made to the recent Ph.D. thesis by Hershey (2). Only a brief survey on the previous work done which is pertinent to the present project is described here.

It appears that B. A. Toms (3) was among the first to notice the abnormal high flow rates of the polymer solutions in circular pipes. The irregularity was observed only in turbulent flow and the transition Reynolds Number remained roughly constant around 2,000. He attributed these results to the wall effects put forward by Oldroyd (4) who suggested that in the immediate neighbourhood of a solid wall, a preferred direction could be introduced into a normally isotropic fluid and in the case of these polymers, an abnormally mobile laminar sublayer might exist and produce an apparent velocity of slip and hence an increase in the flow rate.

Shaver and Merrill (5) performed a large number of tests using various polymers and solution concentrations in different diameters of tubes. Relations between the shear stress and the shear rate for these comparatively high concentration solutions were all represented by the simple power law model, i.e.

$$\tau = b\left[\frac{dU}{dy}\right]^{s} \qquad \text{(II.1)}$$

Plots of the friction factor vs the pseudoplastic Reynolds Number* illustrated that the reduction in drag resistance varied in such a manner that, for a constant Reynolds Number, the friction factor decreased with decreasing values of "s". The velocity profiles were flatter and the mixing lengths calculated were also found to deviate systematically with "s" from that of Newtonian fluids. The dye injection technique was employed to study the mixing processes and they revealed that when the dye was injected at the centre of the tube, it did not disperse as rapidly as it did in a Newtonian fluid. In the case of wall injection, the smoothly flowing layer near the wall was found to be thicker for polymer solutions than for Newtonian liquids, and that the horseshoe vortices formed were relatively few in number and not at all well developed, indicating much lower energy dissipation. They suggested that, since at the centre of the pipe, the shear rate was less than that near the wall, then for a pseudoplastic fluid, the wall region would have a lower viscosity while at the central core, the viscosity would be higher and so the mixing was restrained.

---

* Pseudoplastic Reynolds Number = $\frac{8\rho d^{s} U^{2-s}}{b}\left[2(3 + 1/s)\right]^{-s}$

A thorough theoretical analysis of the turbulent flow of non-elastic, time independent, power law fluids was given by Dodge and Metzner (6). Their experiments on Carbopol, sodium carboxymethy cellulose (CMC), slurries of Attasol and attapulgite clay verified the analysis. It can fairly well be concluded that the general flow phenomena of the pseudoplastic, time independent, purely viscous fluids have been solved. However, in their experiments, they noticed that the friction factor obtained from the solutions of CMC did not agree with their theory. They attributed this deviation to the fact that the CMC possessed viscoelastic properties while the other solutions tested were truly viscous liquids.

In a later paper (7) Metzner, with Park, attempted to take into account this viscoelastic property of a polymer solution. He defined a new parameter which represented the ratio of the elastic to viscous stresses developed by the fluid. The ratio would show the comparative importance of the two stresses, as its value ranged from zero for a purely viscous system towards infinity as the fluid's elasticity increased. Normal stress and friction factor measurements were made on several polymer solutions. The results did seem to agree with the proposed hypothesis but further experiments are required before a definite conclusion can be drawn.

Elata and Tirosh (8) suggested another correlation based on the data of their drag reduction experiments using dilute guar gum solutions. For various concentrations, their data, when plotted

on a graph of $1/\sqrt{C_f}$ vs. $\ln Re_d\sqrt{C_f}$, gave a family of straight lines. Since the slope of such a straight line for a Newtonian liquid is supposed to be inversely proportional to Prandtl's mixing length constant "k", they concluded that "k" was no longer a universal constant. Meyer (9) re-evaluated their work and pointed out that the constant "k" had not changed and that the variation in the slopes was due to a thickening of the laminar and buffer layers near the wall. Ernst's (10) velocity measurements showed that such an explanation could well be correct.

Hershey (2) explained the drag reduction phenomenon by the concept of relaxation times of the polymer solutions. When a Newtonian polymer solution was flowing turbulently, a typical Newtonian friction factor behaviour would be observed provided the relaxation times of the major portion of the polymer molecules were small compared with a time scale characteristic of the flow. If the latter value was smaller, high frequency eddies would transform into low frequency eddies before relaxation could occur. The energy dissipated would then be lower and so causing turbulence suppression and drag reduction.

Virk and co-worker (11) analysed the pipe flow data obtained by several investigators and found that the onset of drag reduction occurred only after the wall shear stress had exceeded a certain

"critical" value. They proposed that the onset of drag reduction should occur at a universal constant value which was defined to be the ratio of the dimensions of the macromolecule in solution and the dissipation wave numbers characteristic of the turbulent flow. The resulting expression obtained indicated that the R.M.S. value of the radius of gyration of the macromolecule was inversely proportional to the critical wall shear stress. Fabula (12) at the same conference as Virk and co-workers presented a paper putting forward several hypotheses in an attempt to explain Tom's Effect. The result of one of these hypotheses was that the R.M.S. value of the radius of gyration of the macromolecule should be inversely proportional to the 3/4 power of the critical wall shear stress. There were not enough data to compare these theories as most previous workers had not measured the solution properties that were required for the above analytical calculations.

Drag reduction measurements have also been obtained for other flow systems. Hoyt and Fabula (13), Hamill (14) and Smallman (1) performed tests with rotating disks. Hamill used only guar gum solutions and the percentage decrease in the torque reached 50% at a concentration of 500 ppm. Smallman used the MRL series in addition to the guar gum series. Kowalski (15) tested the effect of these additives on the frictional resistance of a flat plate and also two ship models. Polymer solutions were injected into the boundary layers of a torpedo shaped body and also a 19 feet

motor boat, and drag reduction of 30 percent and 10 percent respectively were observed.

Hermes and Fredrickson (16) studied the flow of viscoelastic fluids over a flat plate. Due to the large strain rate developed at the leading edge of the plate, the flow behaviour was observed to be quite different from that in a Newtonian fluid. The actual drag force measured was found to be more than twice the value predicted from a purely viscous fluid model, inferring the presence of an elastic effect. Gadd (17) demonstrated some of the visco-elastic effects by squirting a jet of Polyox solution over an inclined plate immersed in the same kind of solution. For pure water the jet spread out but the Polyox jet remained narrow. A transverse pressure measurement across the plate revealed the familiar phenomenon of drag reduction.

In a recent paper Mizushina and Kuriwaki (18) measured the heat transfer coefficients for turbulent flow of pseudoplastic fluids in both a rectangular duct and a circular duct. Temperatures and velocities were measured in order to compute the eddy diffusivities for momentum and heat transfer. Their experimental results were reported to be in good agreement with their derived expressions using the power law model.

II.2 Restrictions on the Use of Velocity Measuring Probes:

In the preceding survey, the velocity distributions had all been measured by immersing a velocity sensitive probe into the flow regime.

Some recent research had revealed that care must be taken in the interpretation of the data obtained in this way. Savins (19), in a paper on the measurement of the first normal stress difference, remarked that the recorded pressure difference (Δp) between an impact tube and a static wall pressure in a laminar Poisuille flow, bore the following relation with the stress deviator of a visco-elastic fluid:

$$(\Delta p)_r = -(P_{11} - P_{22})_r - \int_r^R (P_{22} - P_{33})\, d(\ln r) + \frac{1}{2}\rho U^2 \qquad (II.2)$$

He assumed $P_{22} = P_{33}$ and, denoting the apparent velocity calculated from the Pitot pressure difference by U_{app}, then

$$U_{app} = \sqrt{\frac{2\Delta p}{\rho}} = \sqrt{\frac{2}{\rho}\left[\frac{\rho U^2}{2} - (P_{11} - P_{22})\right]} \qquad (II.3)$$

Thus U_{app} should always be smaller than U. The deviation would only be negligible in the centre of the tube where the shear rate should be zero and became very pronounced as the wall was approached, since the normal stress increased with the shear rate.

Astarita and Nicodemo (20) derived the same equation put forward by Savins. They maintained that the integral term could not be neglected and showed that, for a power law model, the integral term might contribute as much as 80 percent of the dynamic head at the centre of the tube. In their experiments they measured the velocities

both with a Pitot tube and by the actual flow rates. In the eleven test runs the actual collected discharge did not balance with those evaluated from the integration of the velocity distributions. In one run they found that the difference was as high as 30 percent of the actual flow rate.

Metzner and Astarita (21) discussed the change in the deformation rate of a viscoelastic fluid element when it approached the stagnation point of an object and observed that the deformation rate might become so large that the viscoelastic solution might build up a solidlike structure around the tip of the object. The resulting effect would be equivalent to the assumption that the boundary layer developed over the body surface started some distance ahead of the object. To calculate this entended thickness, a relation between the relaxation time and the main stream velocity was derived. For the hot-wire or hot-film probes, an estimation of the order of magnitude of the thickness showed that the liquid film thickness was comparable to, or even greater than, the size of the sensor. This fluid sheath would hence make the probe response very sluggish and thus not only render it useless for high velocities but also make it only valid for time averaged quantities. Moreover, the heat transfer coefficient would become independent of the fluid velocity if the velocity became too high. One way to compensate this was to increase the size of the probe sensor so as to minimize the sheath effect, but then the condition for negligible natural convection would be

violated. Acosta and James and also Leathrum (quoted in Ref. 21) carried out experiments on viscoelastic liquids employing several hot film cylindrical probes of various diameters. The velocity at which the probes became insensitive was very clearly marked by the sharp levelling of the curves, while the magnitude of the threshold velocity at which levelling occurred was found to be of the same order as that calculated from the relaxation time relationship. The same limitations were also applicable to impact tubes and tracer particle studies.

Smith, Merrill and co-workers (22) found that there was good agreement between the velocity profiles obtained by using a Pitot static, Pitot impact and wall static,tap, which, in accordance with both Savins and Astarita, should be considerably different. The effects of the Pitot probe diameter and the main stream velocity on the apparent velocity measured seemed to favour Metzner's theory. Hot film anemometer measurements showed that the heat transfer coefficient was lower in a polymer solution than in pure water. The ratio between these two coefficients began to decrease as the velocity increased. At higher velocities the ratio became discontinuous and fluctuating in character, depicting a highly unstable heat transfer process. The influence of the wall, when a probe was moved near to it during the calibration process, was also noticed.

III EXPERIMENTAL APPARATUS

III.I The Flow System

The experiment was conducted in a tilting flume of a recirculating flow system. Untreated mains water was used which had small quantities of sodium dichromate dissolved in it to reduce metal corrosion within the system. A built-in concrete partition beneath the floor served as the reservoir and an axial single stage centrifugal pump*, driven by a three-phase a.c. motor+, was employed to pump the water from the reservoir to a constant head tank situated about 10 feet above the system .

The overall length of the flume is 40 feet and is supported on an adjustable jack, thus enabling the flume to tilt with respect to the horizontal. The parallel-walled test section of the channel is 30 feet and consists of 5 separate equal sections joined together. Its side walls are panelled with 1/4" thick glass so that visual observation of the flow in the channel is possible. The effective width of the channel is 12" and the maximum allowable liquid depth is around 18". The channel has a smooth metallic floor which has pressure tappings situated along its centre line at equal distances of 1 foot apart. Two parallel straight rails are accurately aligned by set screws on top of the side walls of the channel. This permits carriages, mounted with various

---

* Canada Pumps Ltd., 1400 U.S. gal/min. 1150 r.p.m.
20 ' Head 10 h.p.

\+ Robbins and Myers Co., 3 - Ø , 55 V, 11A, 1140 r.p.m.
10 h.p. continuous duty.

measuring instruments, to traverse freely along the whole length of the flume. The channel has a divergent entrance section which acts as a receiving and plenum chamber for the water discharged from the constant head tank.

The main stream velocity in the channel can be changed by either the gate valve at the entrance section or a tail gate at the end of the flume. The gate valve in effect controls the discharge rate from the constant head tank while the adjustable — height tail gate varies the depth of the water in the channel. The water flows over the tail gate and is directed through drains back into the reservoir underneath.

III.2 The Test Plate

A test plate was designed for this experiment. The working surface is made of a plexiglass plate 4 feet long by 1 foot wide. Two additional plexiglass strips were glued to the underside of the plexiglass plate to give better mechanical strength. 24 pressure holes spaced 2" apart were drilled down the centre line of the plate. In addition two lines of 12 pressure taps of equal spacings were also drilled on each side of the centre line. The 48 pressure holes were fitted, on the underside of the plate ,with short pieces of L shaped stainless steel hypodermic tubes (0.065" O.D.). Long vinyl tubes were used to connect the pressure taps to the pressure measuring apparatus. The bottom of the plate had an aluminum cover to give better flow conditions. Since the polymer solutions were to be

injected into the boundary layer at the leading edge, a separate piece was designed and is described in the next section (III.3).

The support of the plate was constructed in such a way that the plate could be tilted to vary the angle of incidence. The plate was pivoted near the leading edge onto a iron stand resting on the bottom of the channel, whilst two pieces of Dexion perforated angles were fixed to the under side of the plate and protruded 1-1/2" at the rear end. Two screwed brass rods, suspended from a carriage, were pivoted to the ends of the angle irons of the test plate. The depths to which the brass bars come down from the carriage could be adjusted by two nuts on the carriage. Hence, it was possible to vary the angle of incidence of the test plate. In the normal position, i.e. with a zero angle of incidence, the plate surface was about 6" from the bottom of the channel. The plate was located some 16 feet down stream from the entrance of the channel during the experiment.

III.3 Accessories for Polymer Solution Injection

The principal part was a specially designed leading edge piece made of brass. A detailed drawing is shown in Figure IV. The transverse cross section of the leading edge was triangular, and had a 20° angle at one of the vertices which would be the foremost part of the test plate.

The structure was built up by three brass plates joined together on their edges by epoxy cement, while the two ends were

also covered up to form a cavity, which transfered the polymer to the slit. Three short, 1/8" O.D., copper tubes were fitted to the brass plate facing the 20° vortex. The polymer solution was fed into the cavity through these three supply lines. A uniform slot, 1/2" wide and 1/8" deep, was machined across the upper surface of the leading edge piece and a slit, 8" long and 0.02" wide, was cut in the slot to provide a line-source for the polymer solution flowing into the boundary layer. The slot could be fitted with an external brass strip, having a slit of width 0.01", opened just atop the slit in the leading edge piece. Two such strips were made, one having the slit normal, and the other, inclined at an angle of 20° to the surface of the plate.

The supply of the polymer solution was from a measuring tank placed at approximately 10 feet above the level of the injection slit of the test plate. Throughout the experiment, the solution was constantly agitated by a pneumatic stirrer. A plastic tube led the solution down to a regulating needle valve, after which the fluid was diverted and delivered into the cavity within the leading edge piece.

III.4 Measuring Instrumentation

Velocity profiles and turbulence levels were measured using the hot film anemometer technique. The velocity sensitive probes were obtained from two commercial suppliers: the DISA Electronik, Denmark and the Thermo-System Inc., U.S.A. (TSI). Two constant

temperature anemometers* were employed and the turbulence voltage outputs were fed into a random signal indicator and correlator** while the average velocity voltages were supplied to a 2-pen chart recorder+. The hot film probe was fastened to a vertical traversing mechanism which had a vernier gauge such that the position of the probe could be determined to an accuracy of 0.001 ft. The mechanism was fixed to a carriage situated on rails above the channel. Two such arrangements were incorporated so as to measure the correlation coefficient between any two locations in the channel.

It was envisaged that the pressure variation along the plate would be very small and therefore a combination of a pressure transducer*+ with a scani-valve **+ was thought to be more appropriate to pick up the static pressure readings along the plate surface. However, during the preliminary testing stage its performance was found to be unsatisfactory and so the measurement was replaced by a bank of liquid-in-glass manometers. Details of the operation is discussed in the following chapter.

---

* DISA constant temperature anemometer 55A01

** DISA RANDOM SIGNAL INDICATOR AND CORRELATOR 55A06

\+ HONEYWELL Two-pen Electronik 19 Lab. Recorder

*+ Scani-Valve Company PDCR4 $\pm$ 0.2 psid

**+ Scani-Valve Company $48D_3$ - 453

IV EXPERIMENTAL PROCEDURES

IV. 1 Probe Calibration:

Three types of hot-film probes were used in the experiment, the DISA 55A83 and the 1212-60W from the Thermo-Systems Inc., both have their sensors normal to the probes' shanks, while the 1210-60W is a general purpose probe. The overheating ratio was 0.05 in the case of the DISA probe according to its specifications. At first the same ratio was applied in the operation of the TSI probes. However, it soon became clear that at such an overheating ratio the DISA anemometer could not supply enough power to the sensor at the particular velocities being used for calibration. By reducing the ratio to 0.01 the calibration velocity range could be attained by the anemometer and hence forth this value was employed in the subsequent experiments.

The calibration of the probes was carried out in the water channel. The voltage outputs of the probes were plotted against the velocities measured by a Pitot impact tube and the graph was extrapolated to the low velocity range used in the actual experiment. The general calibration equation for a hot film probe is of the form

$$E^2 - E_o^2 = AU^n \qquad \text{(IV.1)}$$

Throughout the research, the temperature of the fluid ranged from 73°F to 77°F depending on the ambient temperature. Though the

values of 'E_o' and 'n' changed slightly it was found to be insignificant when compared to the error invloved in the velocity voltage read out. It had also been noted that occasionally there was a change in the value of the constant 'A'. If 'E_o' and 'n' were assumed to be constant, this would simply result in a parallel vertical shift of the calibration curve in a log.log. plot. Since the main stream velocities used in the experiment were known quite accurately, it meant the voltage corresponding to the main stream velocity had to be determined during each experiment and a separate calibration curve drawn from that point and used in the velocity calculations.

IV.2 Pressure Measurements:

The initial experimental work was to be performed at the zero pressure gradient condition and so the channel was first adjusted to the horizontal position and the plate in turn adjusted. As mentioned before a pressure transducer was initially employed for the measurement of the surface pressure distribution on the plate. The 48 pressure tubings were connected to a scani-valve connector. A 5 volt d.c. motor situated in the scani-valve drove a rotor which transferred these pressures to a pressure transducer and compared to a reference pressure. The difference in the two pressures was expressed as an e.m.f. output. In the trial tests the water was found to flow into the pressure holes on the plexiglass plate in a random manner. Gas bubbles and water pellets of various lengths

were entrained haphazardly. These were quite comparable to the actual pressure differences and so the resulting e.m.f. record-chart was impossible for analysis. The possibility of filling all the tubes with water had been investigated. However, to bleed off all the air inside the system especially at the 48 ports and at the collector duct in the scani-valve proved to be quite difficult with the rather sensitive transducer which was used. Consequently, this method of pressure measurement was temporarily discontinued and substituted by a bank of simple liquid-in-glass manometers. Even so, one or several tappings often showed up erroneous readings mainly due to the tiny gas bubbles entrapped in the tubes. (A vacuum pump was used to suck up the liquid into the U tubes during the experiment but this could not eliminate all the air bubbles in the solution). As the chief objectives of the pressure measurement were to ensure two-dimensional and zero pressure gradient flow, the anomalous readings of these few tappings were ignored.

IV.3 Polymer Solution: Preparation and Injection:

The polymer was dissolved in distilled water and thoroughly mixed with the aid of pneumatic stirrers, usually 24 hours or more before being used for the tests. The concentration was increased as the experiment proceeded so that any residue in the distributing tubes or in the leading edge cavity from the previous experiment would only decrease the concentration. The rate of discharge

was obtained by taking note of the time elapsed during the experiment and the quantity of polymer solution used. The discharge rate could be varied by adjusting the regulating valve. The solution was dyed to observe the injection phenomenon.

When the brass strip with the slit normal to the leading edge surface was employed, back flow phenomenon was frequently observed and the coloured solution dispersed into the main stream very rapidly, probably due to the upward discharge velocity carrying it into the turbulent core of the boundary layer. The case with the inclined slit was very much better; the solution adhered to the plate surface and there was less back flow occurrence. The two flow conditions are compared in the photographs in Fig. V. All the experimental results reported in this thesis were obtained with the 20^{o} injection strip.

IV. 4 Velocity and Turbulence Quantity Measurements:

Since the probes were very sensitive to the fluid temperature, the flow system was allowed to circulate for at least three hours to ensure a uniform fluid temperature before any actual measurement was taken. The sensor resistance was measured for each test run and the voltage corresponding to the main stream velocity was noted. Velocity profile measurements were executed at several locations along the length of the plate. During each traverse into the boundary layer, the voltages for the main stream velocity before and after the traverse were compared to check any drift in

the probe calibration. If there was any significant difference, the entire set of readings were discarded and the traverse repeated again. This occurred most frequently when the polymer solution was injected into the boundary layer. For, in addition to the usual gas bubble formation and contamination of the sensor, polymer molecules would wind around the hot film and affect the normal heat transfer process. Sometimes, the occurrence was indicated clearly by a conspicuous drop in the voltage response and the probe had to be taken out and washed with distilled water.

The velocities in the boundary layer were measured using a TSI 90° probe whose d.c. output voltages were recorded on a continuous chart and were averaged and analysed after the test. The position of the probe was read from the vernier scale on the traversing mechanism. Simultaneously, the mean value of the longitudinal fluctuating velocity component was assessed directly from the DISA correlator.

The two lateral fluctuating velocity components were determined with the aid of a 90° adapter, while the lateral double velocity correlation coefficient was obtained using both the DISA 90° probe and the TSI general purpose probe together. Fig. III-A shows such a set up for the probes. For each position under investigation, the TSI probe was fixed in position while the DISA probe was raised gradually to vary the distance between the probes. The correlation coefficient was read directly from the

DISA correlator.

Owing to the fact that the flow system used was a closed loop, it became inevitable that, after a number of polymer injections, the water in circulation would be slightly contaminated with the polymer molecules. Accordingly, the system was drained, whenever considered necessary, to prevent the concentration from becoming to such a level that it would affect the measurements.

V RESULTS AND DISCUSSIONS

V.I Discussions on Experimental Errors:

The most critical data measurements obtained during the research was the voltage readings from the anemometer output. Due to the unsteady nature of the quantities that were measured and the frequent contamination of the probes, a reasonable degree of accuracy was difficult to achieve. Fig. VI shows a typical d.c. voltage output from the anemometer. The velocity was obtained by averaging the curve visually and then reading off the corresponding value from the calibration curve. If the error in averaging the voltage was 0.1 volt, this would introduce an error in the velocity measurement of as high as 6%. In the vicinity of the plate surface, the error would become still greater as the amplitudes of fluctuations there were enormously high. There was also a problem in determining the true height of the probe sensor from the plate surface. In each boundary layer traverse, the sensor was brought just in contact with the surface by combinations of the feel of the hand and the image of the probe in the plate. However, because of the construction of the probe and the size of the sensor element, there was still a small gap between the sensor and the surface. This finite distance could only be estimated from the dimensions of the sensor and the sensor holder. This fact might explain some of the deviations of the points in the viscous sublayer and the buffer layer.

The static pressure head of the polymer solution at the injection slit was about 12 feet. Usually, in one run, the drop in the liquid level in the supplying tank was less than 3 inches, so that the change in the velocity head would be only 1% and therefore, for all practical purposes, could be assumed to be negligible.

V.2 Velocity Profiles:

Only two main stream velocities were investigated as at higher velocities, vortices were observed to be generated at the entrance of the channel and move down to the test section. The flow Reynolds Number corresponding to the two velocities and based on the length of the plate were 2.4×10^5 and 6.4×10^5. Fig. VII shows the non-dimensional velocity profiles at various locations on the plate, without polymer injection. The universal logarithmic law and the equation for the viscous sublayer were plotted on all the graphs where applicable.

$$U^+ = A_1 \text{ Log } y^+ + B \qquad (V.1)$$

$$U^+ = y^+ \qquad (V.2)$$

The constants in Eq.(V.I) were obtained from reference (23), where $A_1 = 5.85$ and $B = 5.56$. It can be seen that there was good agreement between the experimental data and the log. law plot. This good agreement showed that the equipment was functioning well. Water was injected at two different rates into the boundary layer to act as a control test. Figure VIII shows the resulting velocity profiles

and again, there was not much deviation from the standard profiles.

Figures IX to XV illustrate the development of the velocity profiles at various stations under various injection conditions. The distances normal to the plate surface had been non-dimensionalized with respect to the boundary layer thickness of pure water at the same Reynolds Numbers, instead of with respect to their own boundary layer thickness. This is because the evaluation of these values from the experimental points is quite difficult. Also, it is thought that, when expressed in the present form, the development of the velocity profiles can be best envisioned. These graphs showed that for a short distance from the slit the polymer solution was slowly dispersing and gaining speed. Further down the plate, the viscoelastic properties of the polymer solutions appeared to come into play and give rise to the fuller profiles. The magnitudes of these effects were consistent with respect to the discharge rates and the concentrations. This trend of variation would follow immediately if we make the plausible assumption that, in a polymer solution, the higher the concentration, the higher its inertia will be, and, therefore, the longer time it will take to be accelerated and completely mixed.

In calculating the velocities, the calibration curves for pure water had been used even when there was polymer solution injection. The main reason is that there is, at present, no easy way of determining the concentrations or concentration gradients of the

polymer solution in the boundary layer, which meant that, even if the probe was calibrated at various concentrations, there would still be no way of applying these curves in the calculations. In the experiment, the velocity was very low and the maximum concentration, assuming uniform mixing, in the boundary layer was less than 3 p.p.m. Hence, the discussions in references (21) and (22) on the restrictions in the using of the hot-film probes would most probably not apply in the present situation.

V.3 Drag Reduction

Since the momentum thickness of a boundary layer is a measure of the drag force at a certain position, and that the fuller the velocity profile, the shorter will be its momentum thickness, therefore, comparing the shapes of the velocity profiles with and without polymer injection, the effect on the drag force could be inferred from the "fullness" of the profiles. In figures IX to XV it could be seen that drag reduction occurred at the rear part of the plate. Though the velocity gradients at the wall seemed to remain approximately the same, higher confidence should be placed on the data obtained in the outer region, where the fluctuations in the voltage outputs were not so severe as at the wall, and thus more reliable. The four cases where drag reduction had taken place were calculated from the momentum thicknesses.* A sample calculation is presented in Appendix I. The reduced wall shear stress were evaluated in order to compute the non-dimensional

---

* When the polymer solution boundary layer is thinner, drag reduction is considered to have taken place.

quantities U+ and Y+, the results of which are plotted in Figure XVI. Some data points from reference (10) are also shown for comparison. From the graphs it looks as if only the value 'B' in equation (V.1) has increased. However, it was noted in reference (12) that the apparent parallel upward shift of the curves could not eliminate the possibility of a change in the slope in equation (V.1); more data are required to support such an assertion. At present, it suffices to say that the viscous sub-layer and the buffer layer seem to have become thicker in a visco-elastic fluid. The possibility of a change in the slope and in its transport mechanism will be discussed fuller in the following section (V.4).

V.4 Turbulence Intensities and Integral Scales:

The turbulence intensities relative to the local mean velocities in the three directions are illustrated in Figures XVII and XVIII. The two lateral components are each relatively higher than the conventional results as given in reference (24). This probably arose from the rather crude approach used in the present experiment. From the graphs, it could be said that, as a first approximation, the outer part of the boundary layer was isotropically turbulent. There was a small decrease in the turbulence levels close to the plate surface when polymer solutions were injected while practically the same turbulence was observed in the rest of the flow regime. These measurements were all taken at the end of the plate where the solution

was assumed to be already fairly well mixed. It is therefore concluded that greater suppression would be obtained if higher concentrations were used. The decrease in the turbulence kinetic energy suggested that the frequencies of the dissipative eddies had decreased. This would mean that there was an increase in the average size of the eddies responsible for energy dissipation. The observations are in general agreement with the discussions in (2,5,12,17, 25).

The measurements of the lateral correlation coefficients in the boundary layer are shown in Figures XIX and XX. Because of the configurations of the probes, it was not possible, in the present work, to obtain data for the region $r \leq 0.003$ ft. From the curves the lateral integral scales were computed by numerical integration. In Appendix II, it is shown that in a homogeneous isotropic turbulence field,

$$L_f = 2\, Lg \qquad (V.3)$$

From the above equation, the longitudinal integral scales were calculated. The values thus obtained are very much the same as those given in reference (26) which were calculated from the energy spectra.

The integral scales could also be viewed as a measure of the average size of the largest eddies. In the presence of the polymer solutions, the integral scales were reduced signifying a decrease

in the size of these eddies. Hence the effect of the polymer solution seems to bring the eddies in a turbulence field to a more uniform size.

Figure XXI shows the distribution of the eddy viscosity across the boundary layer. The points with no injection compare fairly well with Klebanoff and Townsend's data (24). When polymer solution was injected, the values were smaller and more scattered. In reference (25) it was found that the heat transfer was lower in a viscoelastic liquid. It appears that the eddy diffusivities for momentum, heat and probably also for mass transfer are lower in a viscoelastic liquid. The slope at the origin gives the value of the mixing length constant k = 0.4. Shaver (5) measured the mixing lengths of pseudoplastic fluids and found that the value of "k' had changed. In the present work, the points are too few to permit any rigorous conclusion.

VI CONCLUSIONS

As a summary to the previous discussions, the following conclusions can be drawn:

(1) Drag reduction was observed as expected, but there was an increase in drag resistance immediately after the injection slit. The latter effect may be diminished by applying a higher rate of injection.

(2) The viscoelastic properties of the polymer solution seem to promote a more uniform distribution of the sizes of the turbulence eddies.

(3) The eddy viscosity of a viscoelastic liquid is smaller than that of a Newtonian viscous liquid.

VII RECOMMENDATIONS

In view of the measuring difficulties, some type of data acquisition system, which could continuously record data and analyze it more accurately and conveniently at a later time, would be most suitable for the future work in this field. New methods of velocity measurements in viscoelastic fluids, void of the restrictions discussed earlier, should be thoroughly investigated. To study the flow mechanisms of these viscoelastic fluids, a given concentration solution in a closed-loop system would yield more fruitful results than the present injection method.

On the other hand, in order to study the practicability of the drag reduction effect, by the polymer solutions on ships, the installation of a drag force measuring balance, to evaluate the overall drag reduction effect on a submerged body, is highly recommended. Various rates of injection for different solution concentrations should be applied to obtain an optimum drag reduction effect. It was known that continuous injection into the boundary layer is both uneconomical and impracticable. Hence, other techniques of injection, e.g. in pulses, at several locations over the entire body surface or at points where transition or separation are pending should be investigated.

VIII REFERENCES

1. Smallman, J. R.: "The Influence on Hydrodynamic Drag of High Molecular Weight Compounds in the Turbulent Boundary Layer", M. Eng. thesis, McMaster University, 1967.

2. Hershey, H. C.: "Drag Reduction in Newtonian Polymer Solutions", Ph.D. thesis, University of Missouri at Rolla, 1965.

3. Toms, B. A.: Proceedings of the International Rheological Congress, Schevenigen, Holland, 1948.

4. Oldroyd, J. G.: ibid

5. Shaver, R. G. and E. W. Merrill,: A.I.Ch.E. Journal, Vol. 5, No.2, June 1959, p. 181.

6. Dodge, D. W. and A. B. Metzner,: A.I.Ch.E. Journal, Vol. 5, No. 2, June 1959, p. 189.

7. Metzner, A. B. and M.G.J. Park: J. Fluid Mechanics, Vol. 20, 1964, p. 291.

8. Elata, C. and J. Triosh: Israel Journal of Technology, Vol. 3, No. 1, 1965, p. 1.

9. Meyer, W. A.: A.I.Ch.E. Journal, Vol 12, No. 3, May 1966, p. 522.

10. Ernst, W. D., ibid, p. 581.

11. Virk, P.S., E. W. Merrill, H. S. Mickley, and K. A. Smith: Proceedings of the International Rheological Congress, Syracuse University, N. Y., 1965, p. 37.

12. Fabula, A. G., T. L. Lumley and W. D. Taylor: ibid, p. 145.

13. Hoyt, J. W., A. G. Fabula: "Frictional Resistance In Towing Tanks", 10th I.T.T.C., Sept., 1963.

14. Hamill, P. A.: Internal Memorandum, N.R.C., Canada, No. MTB-65, April 1964.

15. Kowalski, T.: Naval Engineer Journal, April 1966, p. 293.

16. Hermes, R. A. and A. G. Fredrickson: A.I.Ch.E. Journal, Vol. 13, No. 2, March 1967, p. 253.

17. Gadd, G. E.: Nature, No. 4983, May 1st, 1965, p. 463.

18. Mizushina, T. and Y. Kuriwaki: Memoirs of the Faculty of Engineering, Kyoto University, Vol. XXIX, Part 2, April 1967, p. 197.

19. Savins, J.G.: A.I. Ch.E. Journal, Vol. 11, No. 4, July 1965, p. 673.

20. Astarita, G. and L. Nicodemo: A.I.Ch.E. Journal, Vol. 12, No. 3, May 1966, p. 478.

21. Metzner, A.B. and G. Astarita: A.I.Ch.E. Journal, Vol. 13, No. 3, May 1967, p. 550.

22. Smith, K. A., E. W. Merrill, H. S. Mickley and P. S. Virk: Chem. Eng. Sci., Vol. 22, 1967, p. 619.

23. Schlichting, H.: "Boundary Layer Theory". McGraw-Hill Book Co. 4th edition.

24. Hinze, J. O.: "Turbulence,An Introduction to Its Mechanism and Theory". McGraw-Hill Book Co.

25. Gupta, M. K., A. B. Metzner and J. P. Hartnett: Int. Jour. of Heat and Mass Transfer, Vol. 10, No. 9, Sept. 1967.

26. Patterson, G. K., J. L. Zakin: A.I.Ch.E. Journal, Vol. 13, No. 3, May 1967, p. 513.

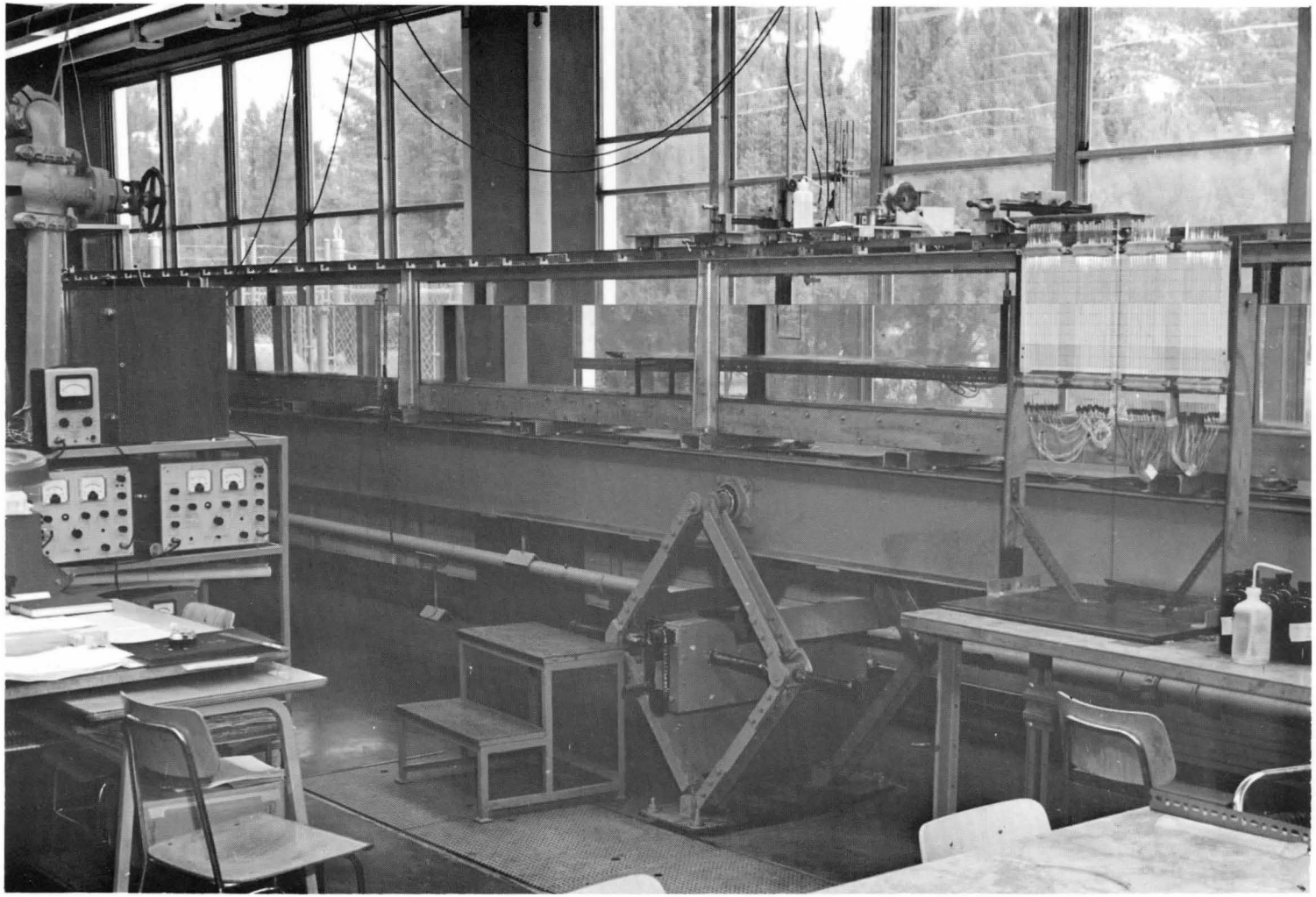

GENERAL VIEW OF THE POLYMER INJECTION FLAT PLATE MODEL SET-UP

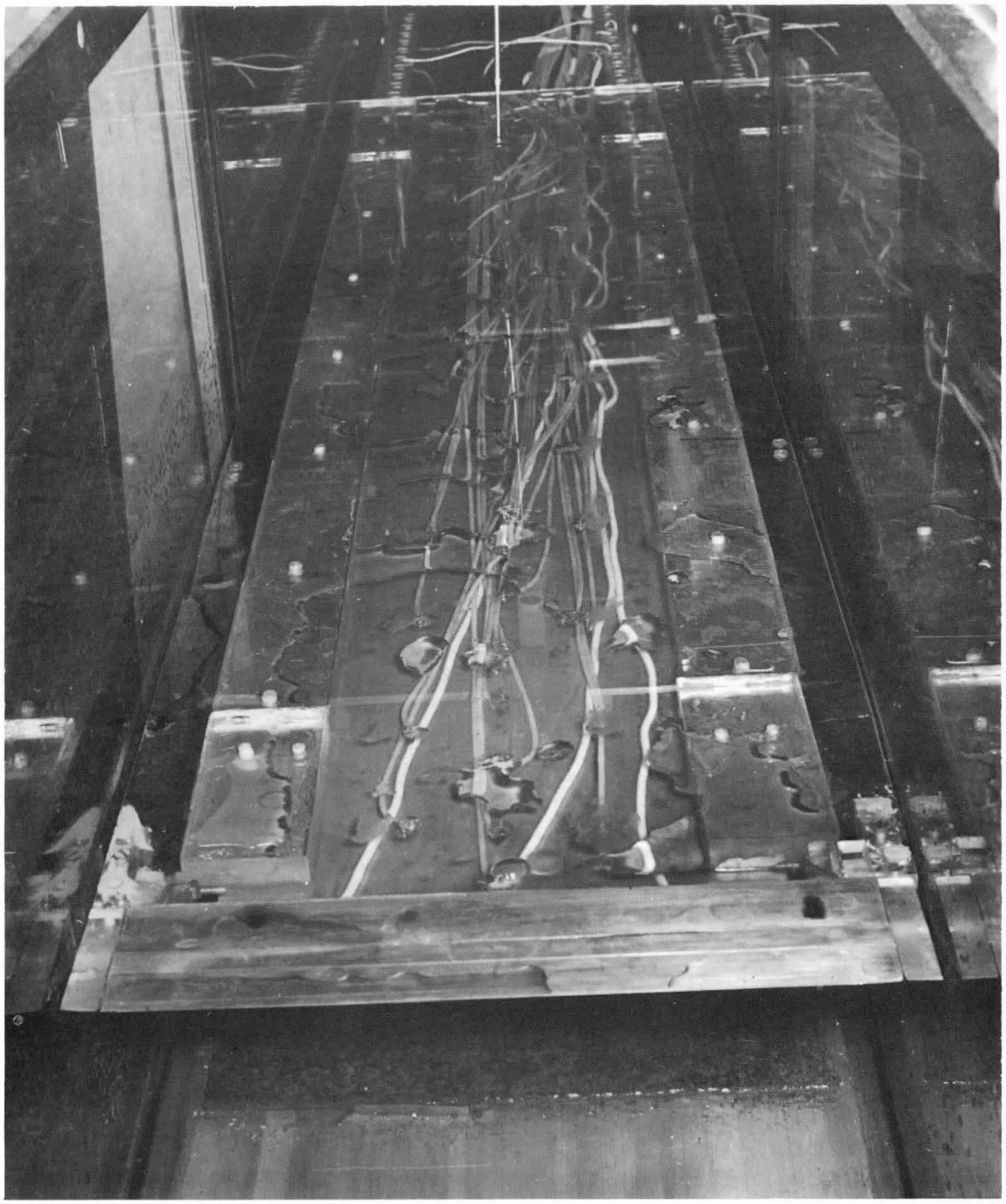

TOP VIEW OF POLYMER INJECTION MODEL
(THE PRESSURE TAPS CAN BE SEEN BELOW
THE PLEXIGLASS PLATE SURFACE)

VIEW OF THE ANEMOMETER PROBES
(TURBULENCE SCALE MEASUREMENT)

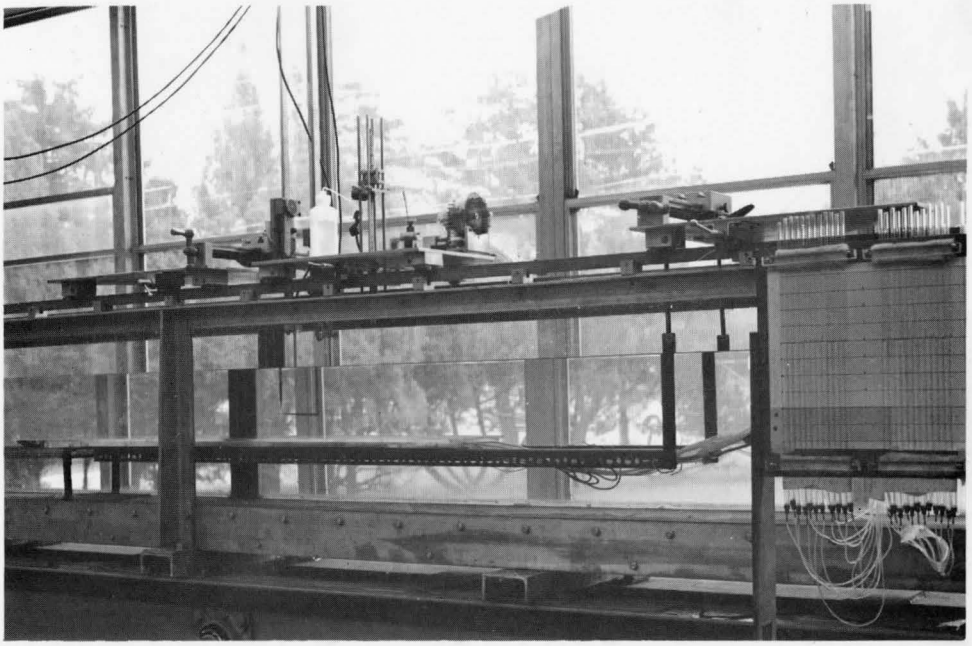

POLYMER INJECTION FLAT PLATE MODEL

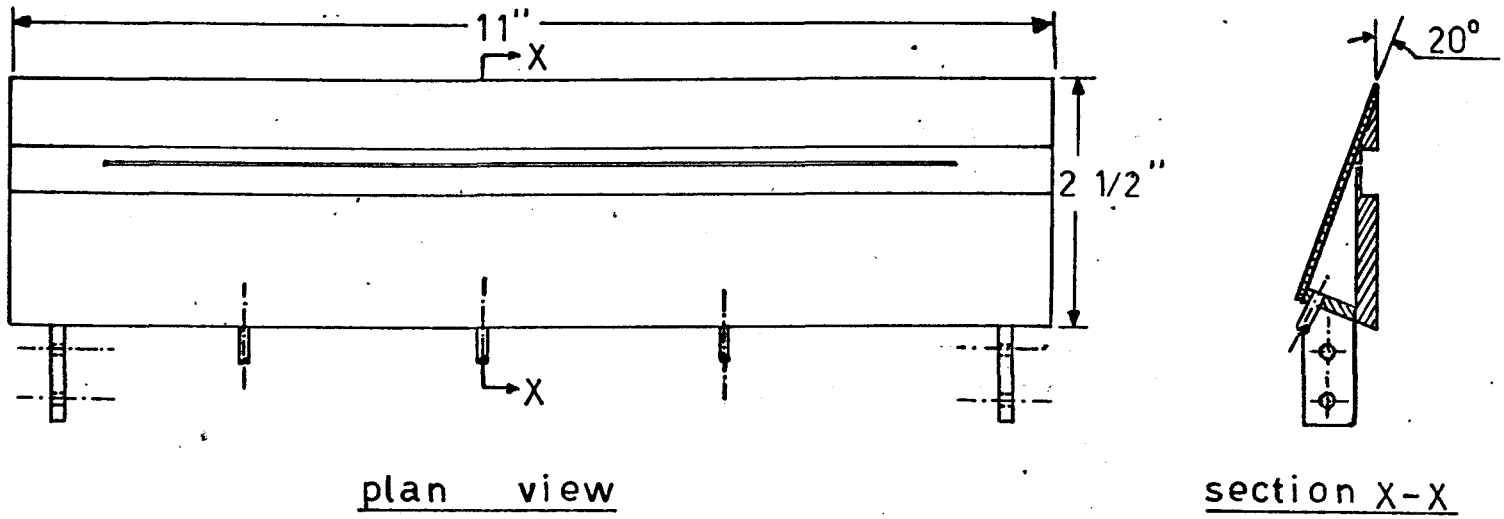

FIG. IV—THE LEADING EDGE PIECE

Scale 1/2 : 1

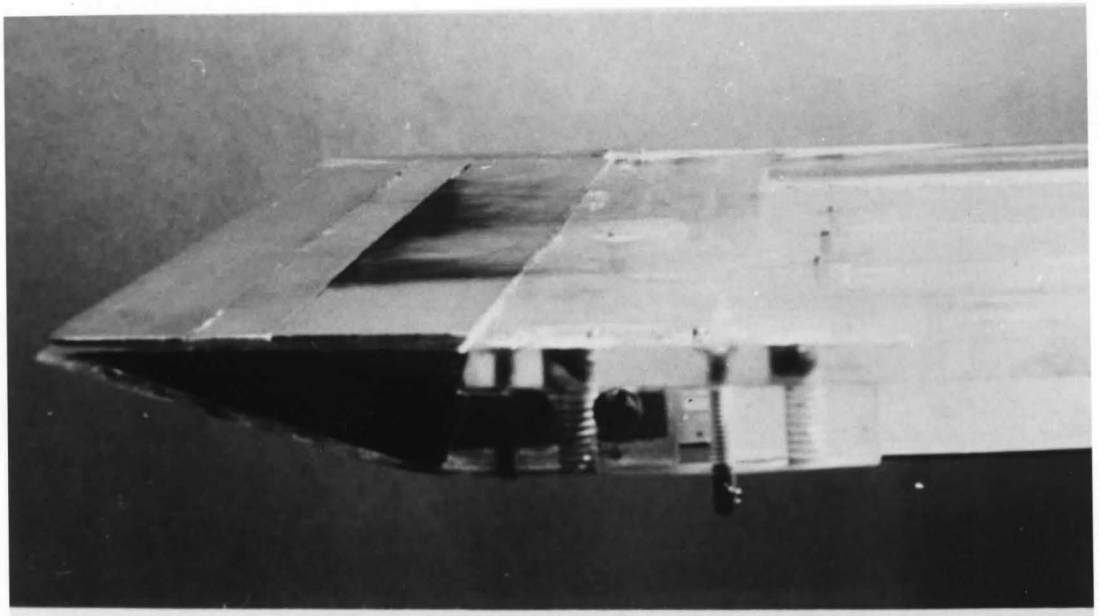

FIG. V-A—POLYMER SOLUTION INJECTION THROUGH A 20° SLIT

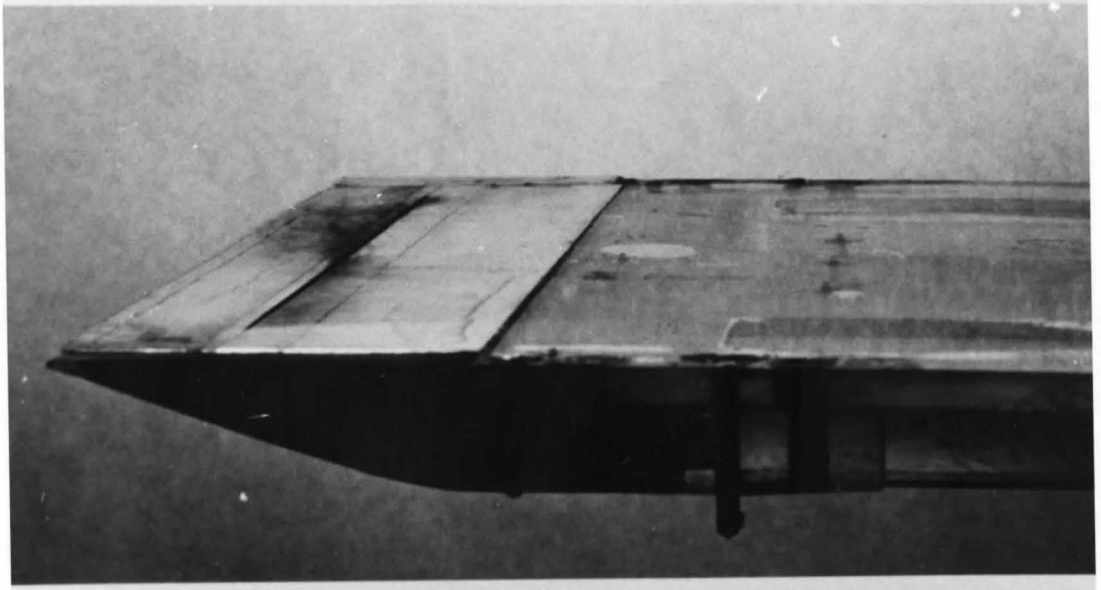

FIG. V-B—POLYMER SOLUTION INJECTION THROUGH A 90° SLIT

FIG. VI—A TYPICAL ANEMOMETER VOLTAGE OUTPUT FOR THE MEASUREMENT OF AVERAGE VELOCITY

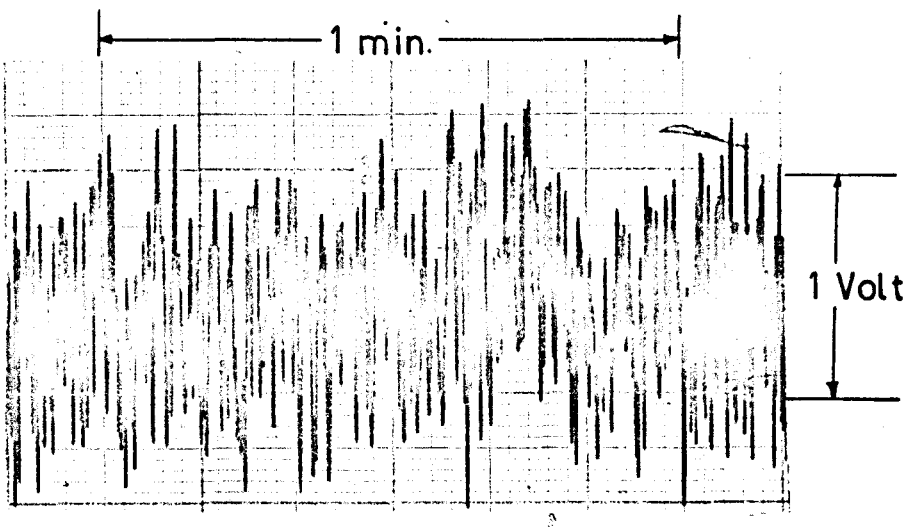

IN THE VISCOUS SUBLAYER

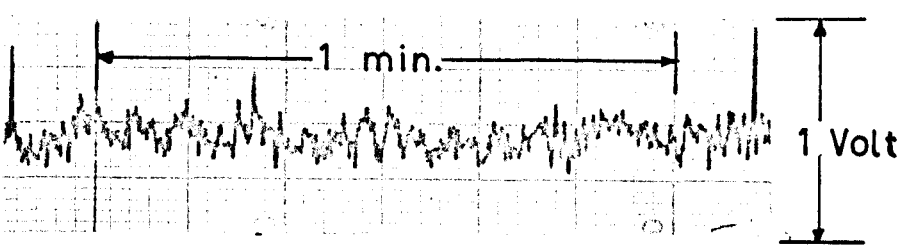

IN THE MAIN STREAM

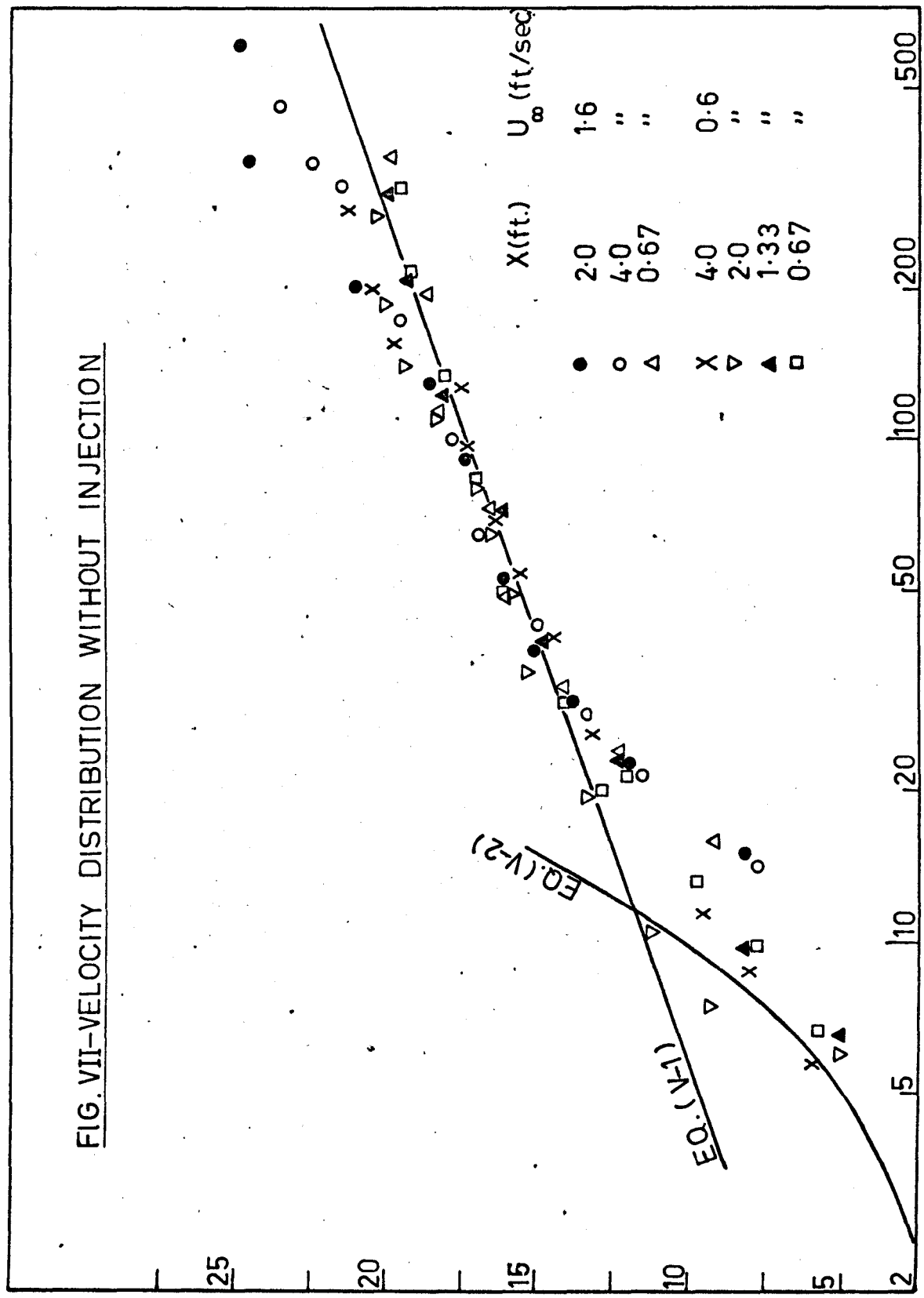
FIG. VII-VELOCITY DISTRIBUTION WITHOUT INJECTION
U+
Y+
EQ.(V-1)
EQ.(V-2)
X(ft.)
U∞ (ft/sec)
2·0
4·0
0·67
4·0
2·0
1·33
0·67
1·6
0·6
2
5
10
15
20
25
50
100
200
500

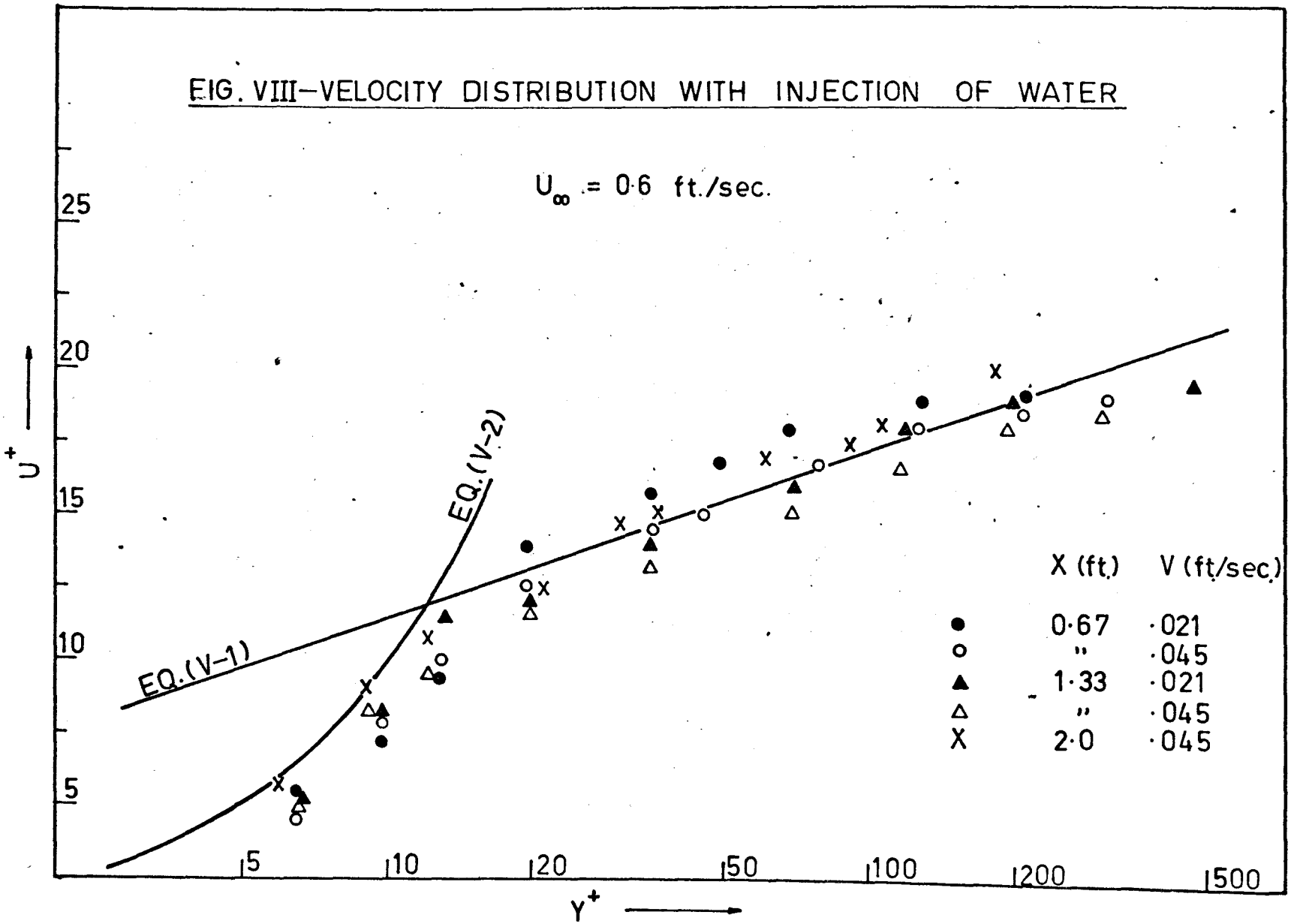
FIG. VIII—VELOCITY DISTRIBUTION WITH INJECTION OF WATER
U_∞ = 0·6 ft./sec.
U^+
Y^+
25
20
15
10
5
5
10
20
50
100
200
500
EQ.(V-1)
EQ.(V-2)
X (ft.)
V (ft/sec.)
0·67
·021
"
·045
1·33
·021
"
·045
2·0
·045

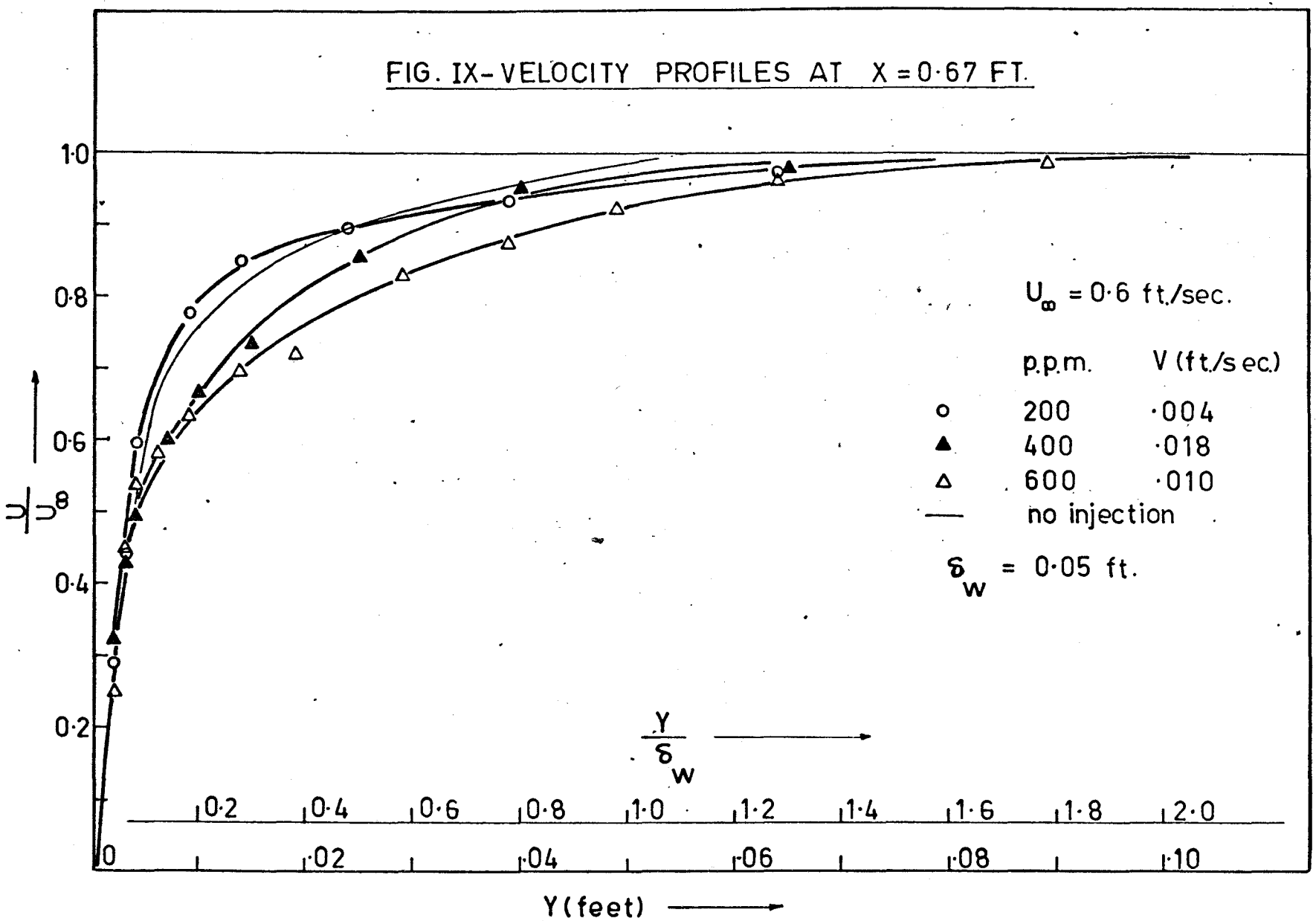
FIG. IX- VELOCITY PROFILES AT X = 0·67 FT.
1·0
0·8
0·6
0·4
0·2
U/U∞
U∞ = 0·6 ft./sec.
p.p.m.
V (ft./sec.)
200
·004
400
·018
600
·010
no injection
δw = 0·05 ft.
Y/δw
0·2
0·4
0·6
0·8
1·0
1·2
1·4
1·6
1·8
2·0
0
·02
·04
·06
·08
·10
Y (feet)

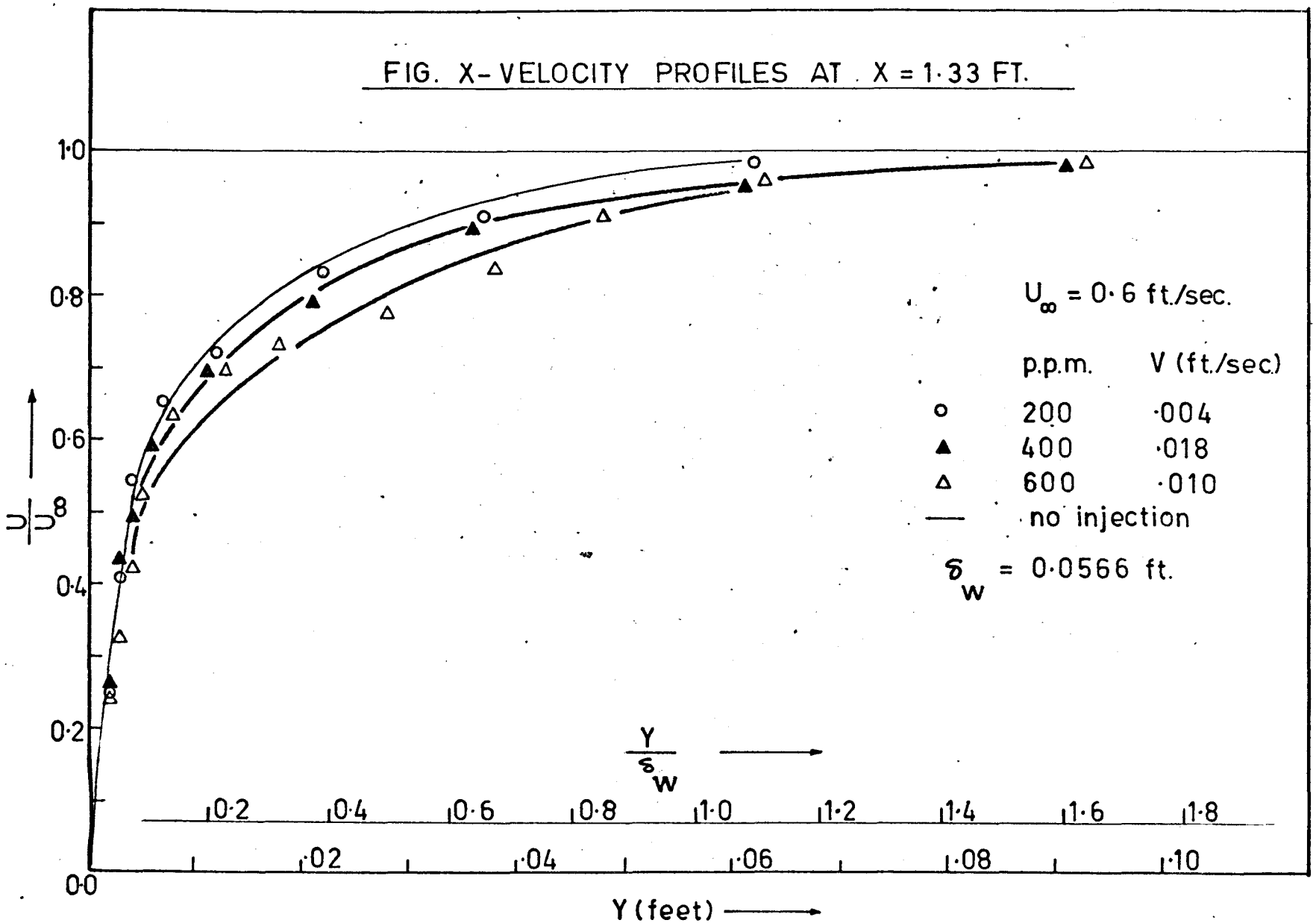
FIG. X- VELOCITY PROFILES AT X = 1·33 FT.
1·0
0·8
0·6
0·4
0·2
0·0
U/U∞
U∞ = 0·6 ft./sec.
p.p.m. V (ft./sec.)
200 ·004
400 ·018
600 ·010
no injection
δw = 0·0566 ft.
Y/δw
0·2 0·4 0·6 0·8 1·0 1·2 1·4 1·6 1·8
·02 ·04 ·06 ·08 ·10
Y (feet)

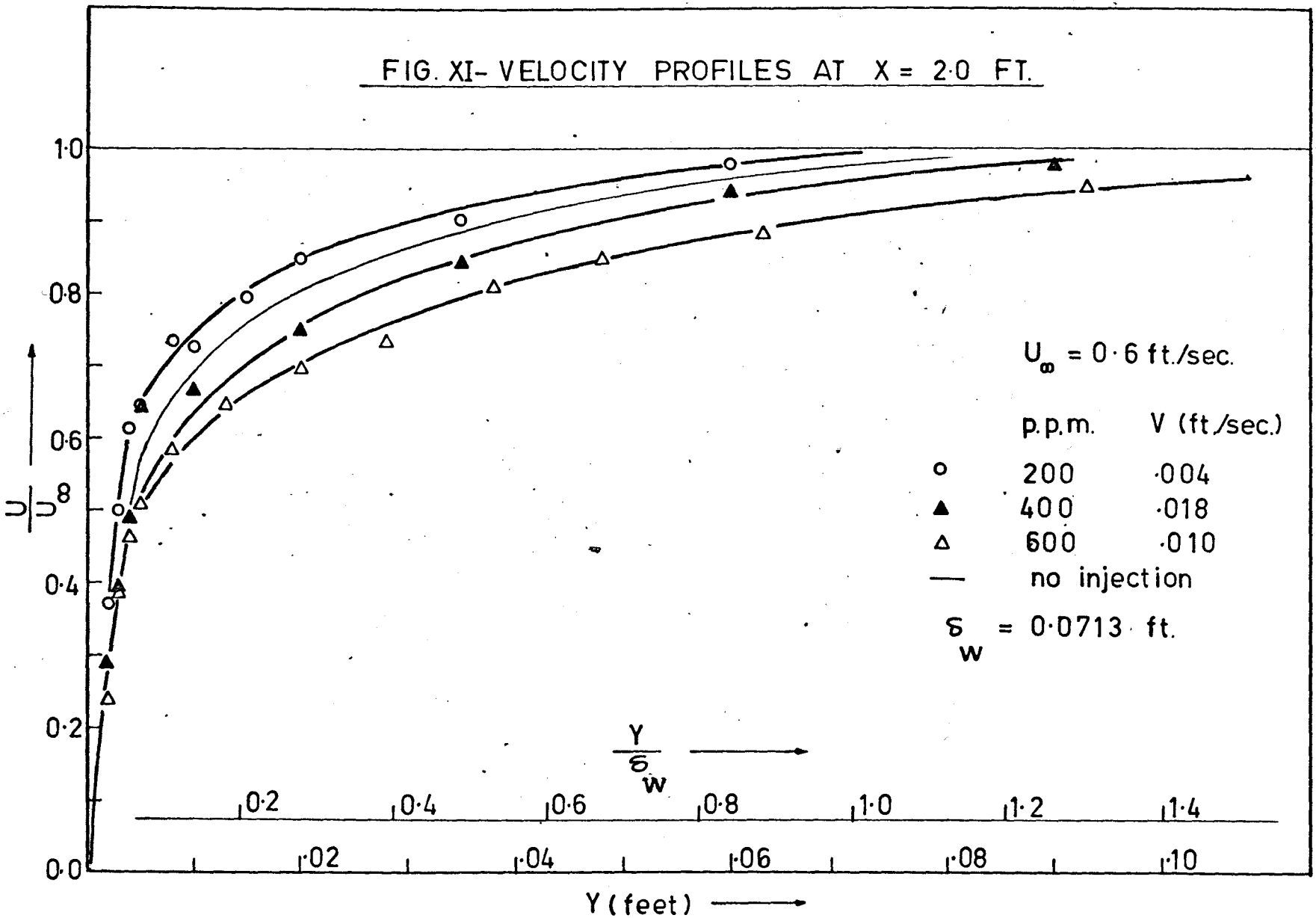
FIG. XI- VELOCITY PROFILES AT X = 2·0 FT.
1·0
0·8
0·6
0·4
0·2
0·0
U/U∞
U_∞ = 0·6 ft./sec.
p.p.m. V (ft./sec.)
200 ·004
400 ·018
600 ·010
no injection
δ_w = 0·0713 ft.
Y/δw
0·2 0·4 0·6 0·8 1·0 1·2 1·4
·02 ·04 ·06 ·08 ·10
Y (feet)

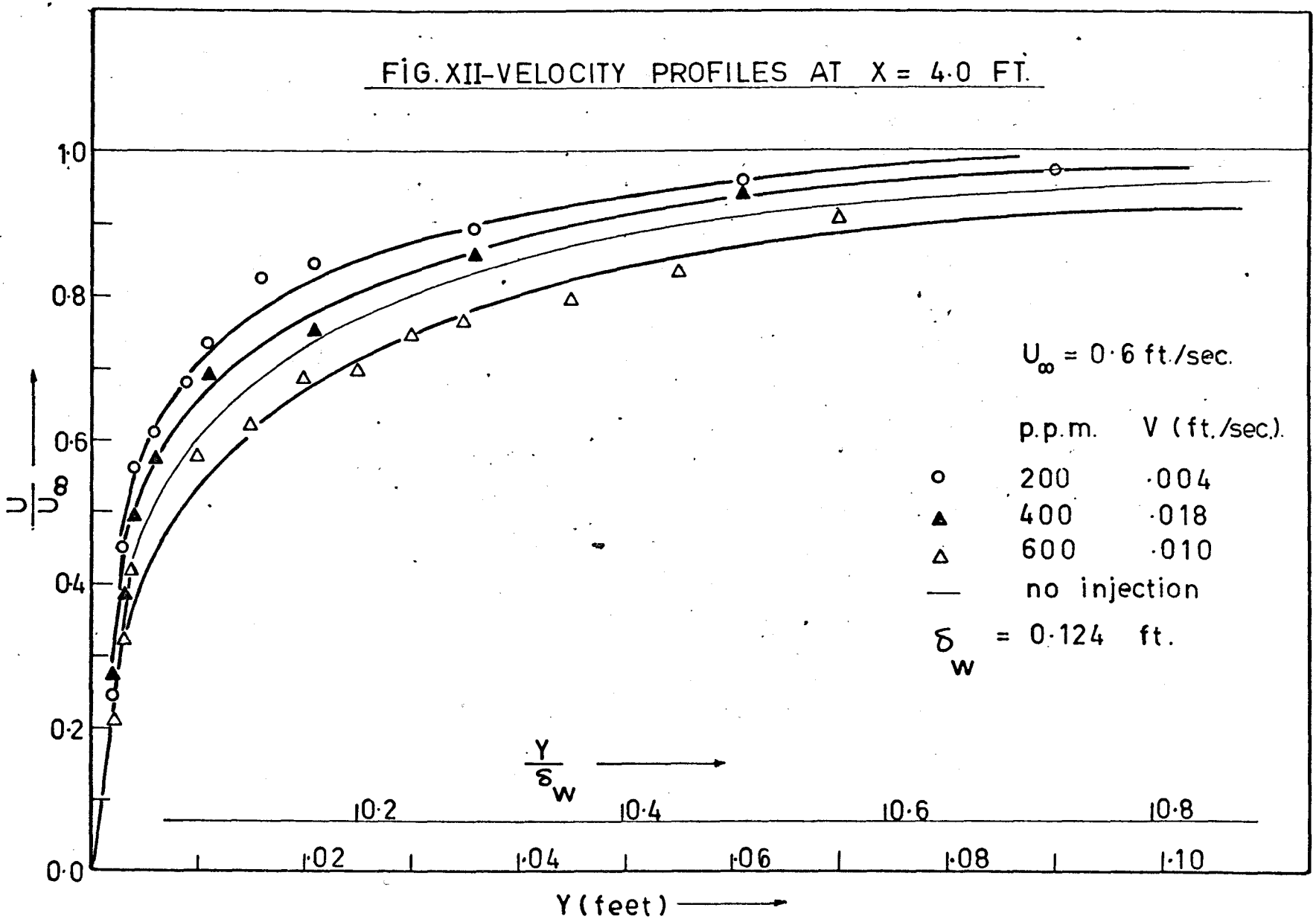
FIG. XII-VELOCITY PROFILES AT X = 4·0 FT.
1·0
0·8
0·6
0·4
0·2
0·0
U/U∞
U∞ = 0·6 ft./sec.
p.p.m. V (ft./sec.)
200 ·004
400 ·018
600 ·010
no injection
δw = 0·124 ft.
Y/δw
0·2
0·4
0·6
0·8
·02
·04
·06
·08
·10
Y (feet)

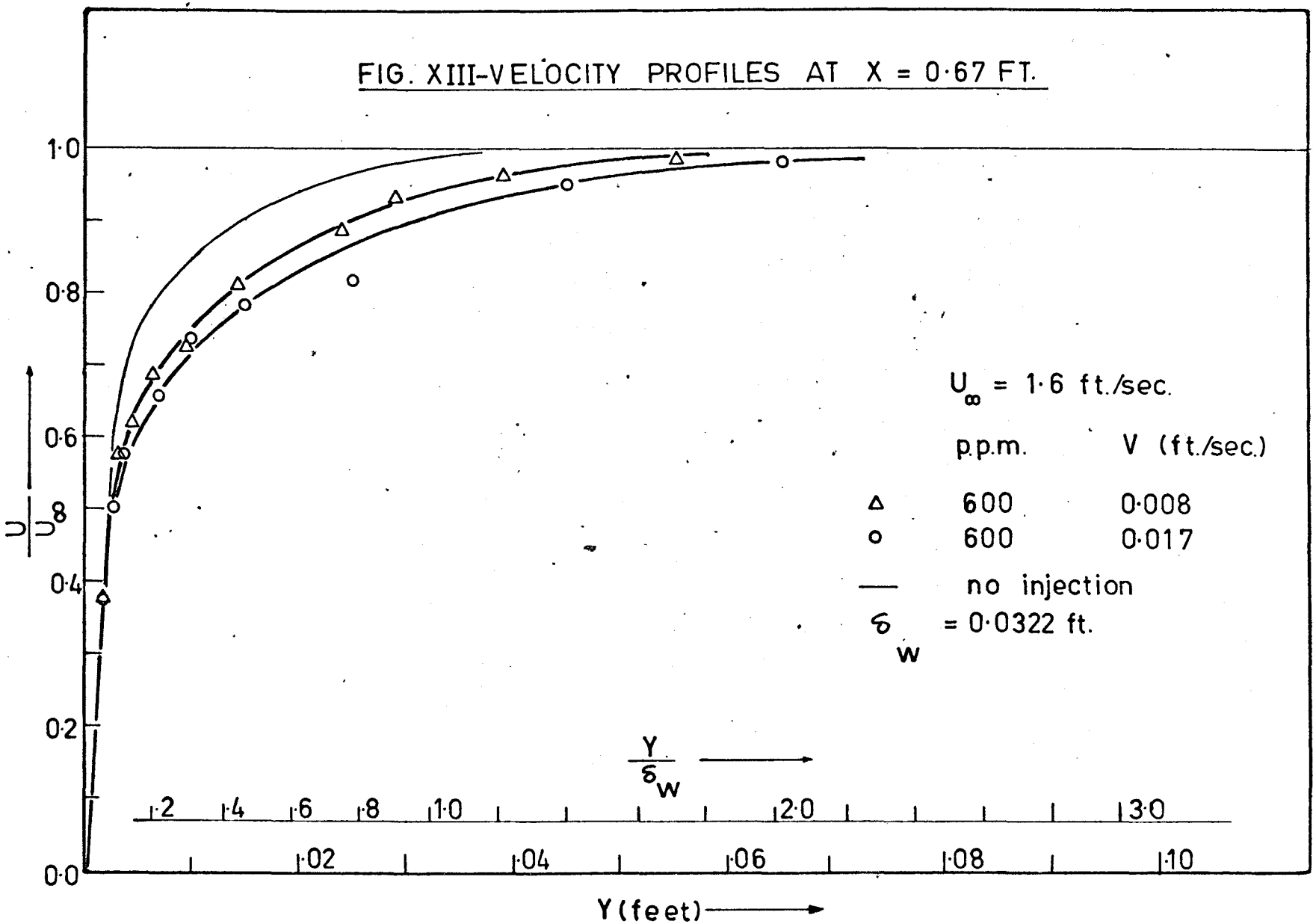
FIG. XIII-VELOCITY PROFILES AT X = 0·67 FT.
1·0
0·8
0·6
0·4
0·2
0·0
U/U∞
U∞ = 1·6 ft./sec.
p.p.m.
V (ft./sec.)
600
0·008
600
0·017
no injection
δw = 0·0322 ft.
Y/δw
·2
·4
·6
·8
1·0
2·0
3·0
·02
·04
·06
·08
·10
Y (feet)

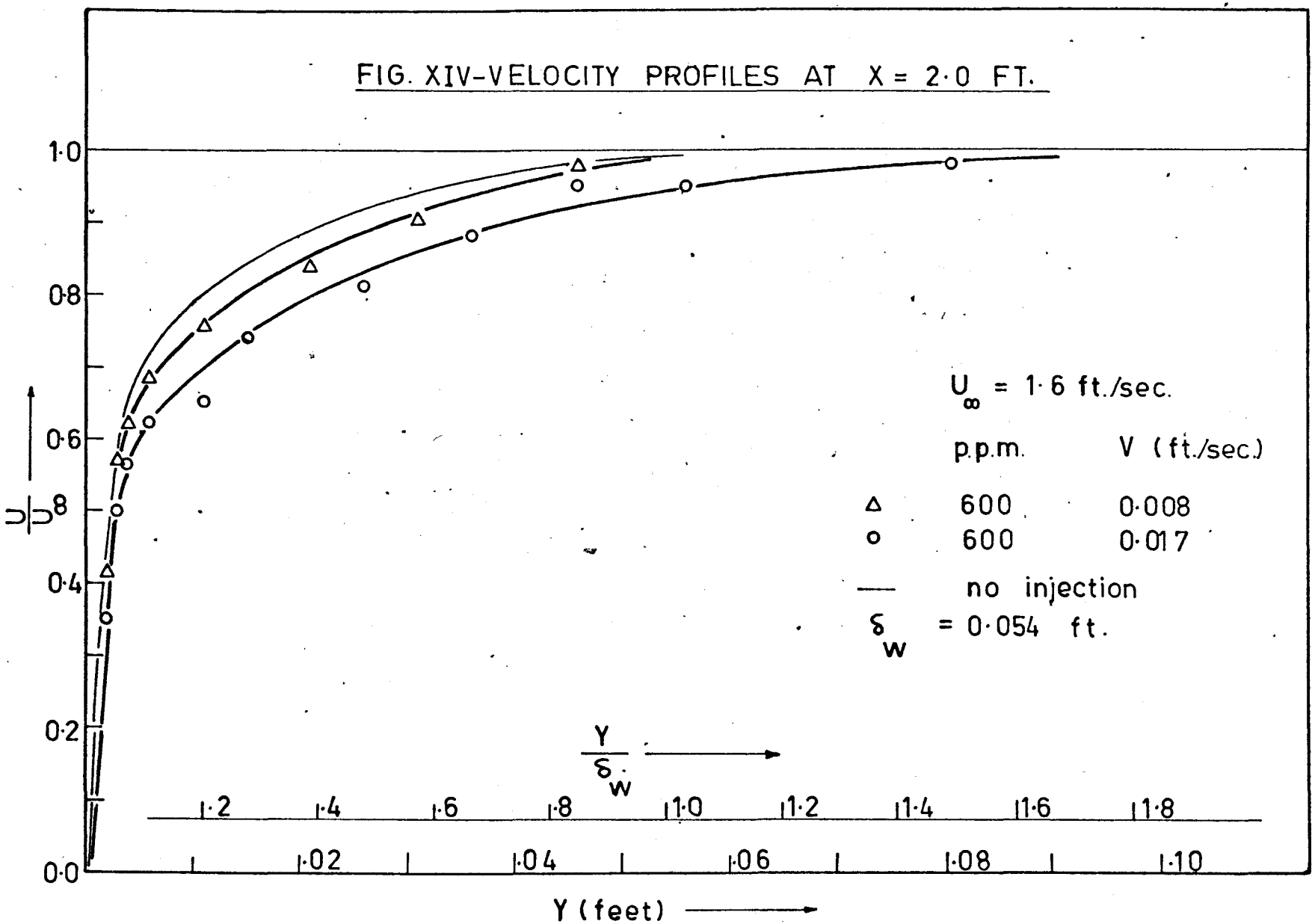
FIG. XIV-VELOCITY PROFILES AT X = 2·0 FT.
1·0
0·8
0·6
0·4
0·2
0·0
U/U∞
U∞ = 1·6 ft./sec.
p.p.m.
V (ft./sec.)
600
0·008
600
0·017
no injection
δw = 0·054 ft.
Y/δw
·2
·4
·6
·8
1·0
1·2
1·4
1·6
1·8
·02
·04
·06
·08
·10
Y (feet)

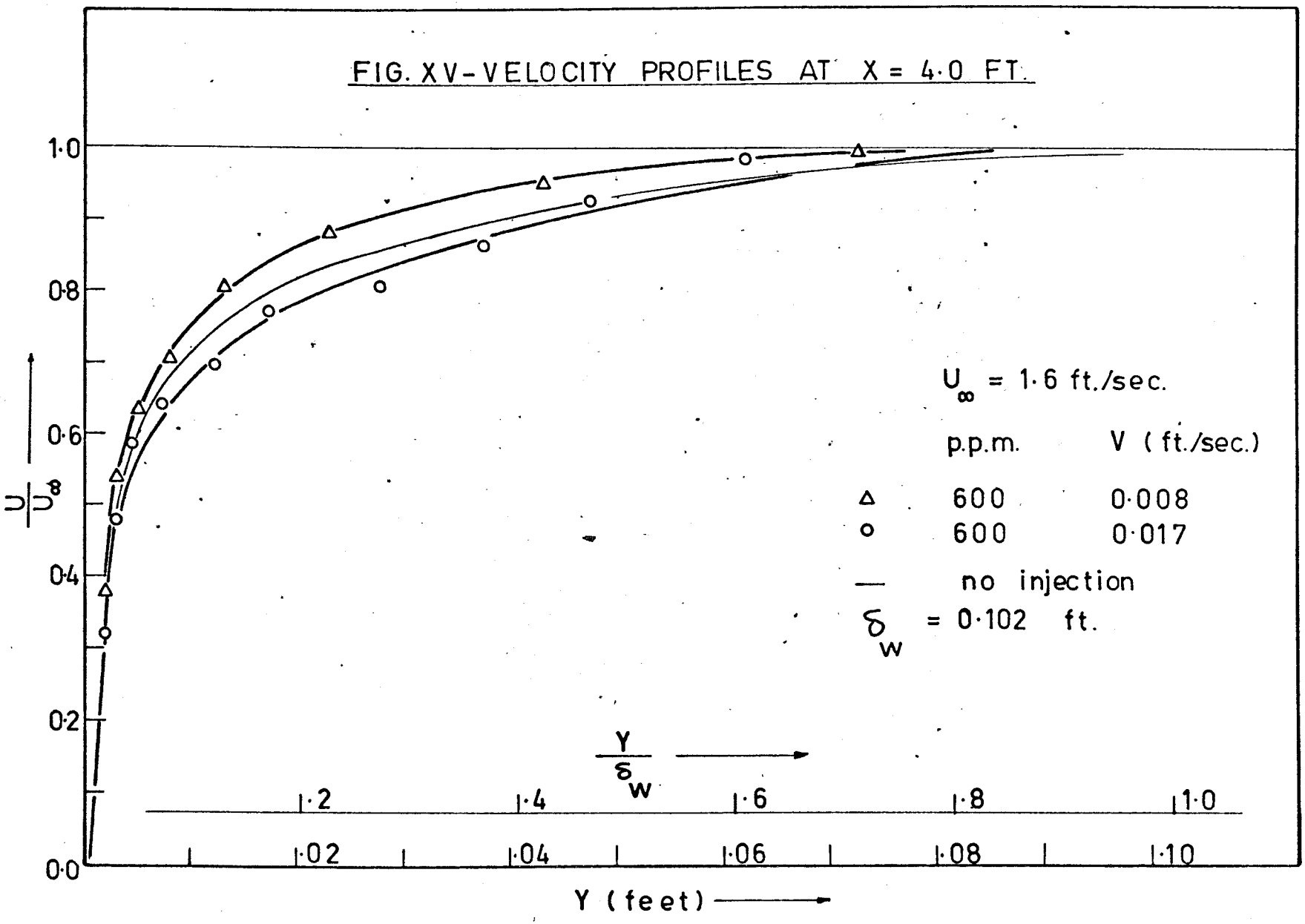
FIG. XV - VELOCITY PROFILES AT X = 4·0 FT.
1·0
0·8
0·6
0·4
0·2
0·0
U/U∞
U∞ = 1·6 ft./sec.
p.p.m.
V (ft./sec.)
600
0·008
600
0·017
no injection
δw = 0·102 ft.
Y/δw
·2
·4
·6
·8
1·0
·02
·04
·06
·08
·10
Y (feet)

FIG. XVI – VELOCITY DISTRIBUTION WITH INJECTION OF POLYMER SOLUTIONS

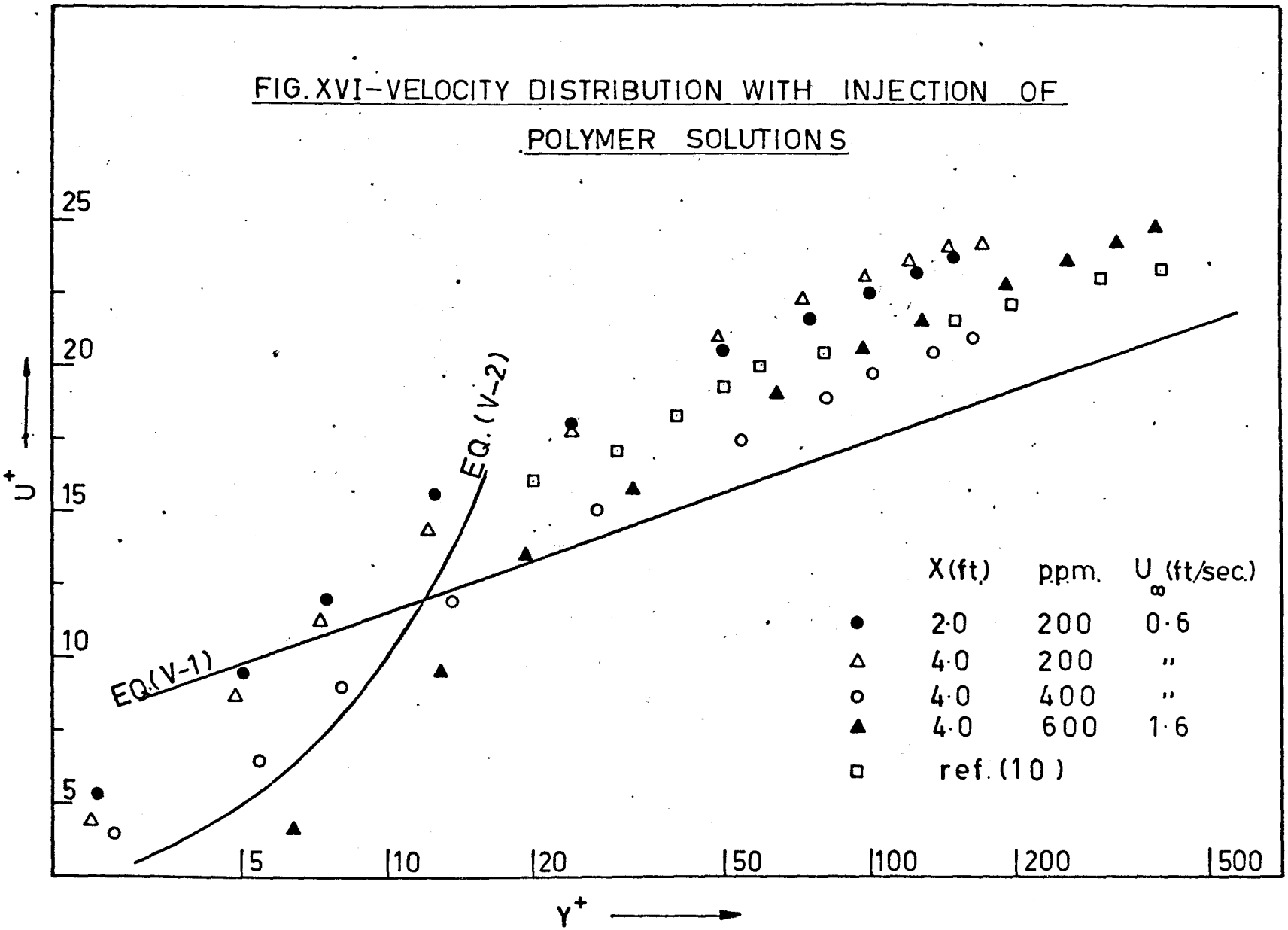

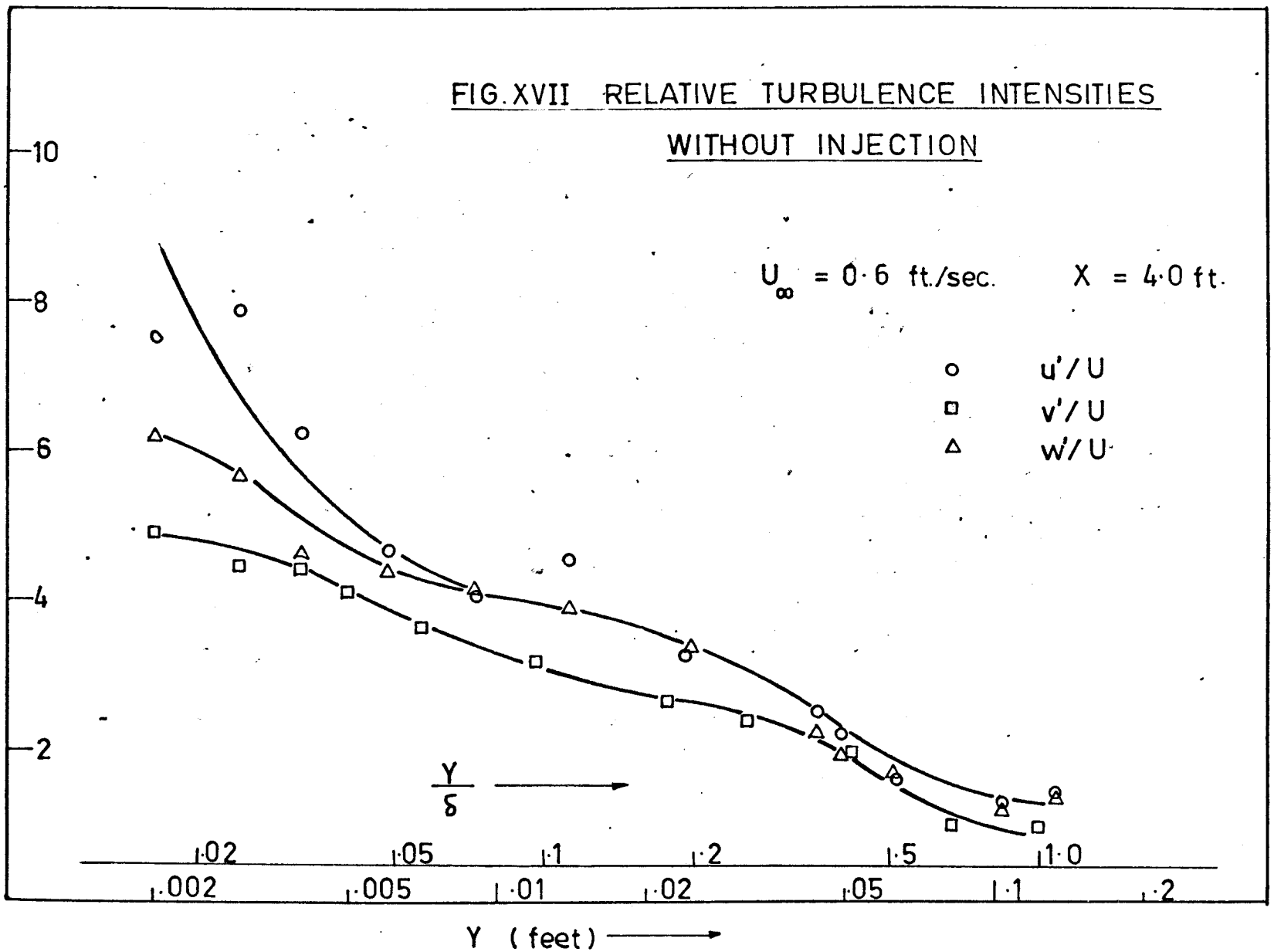

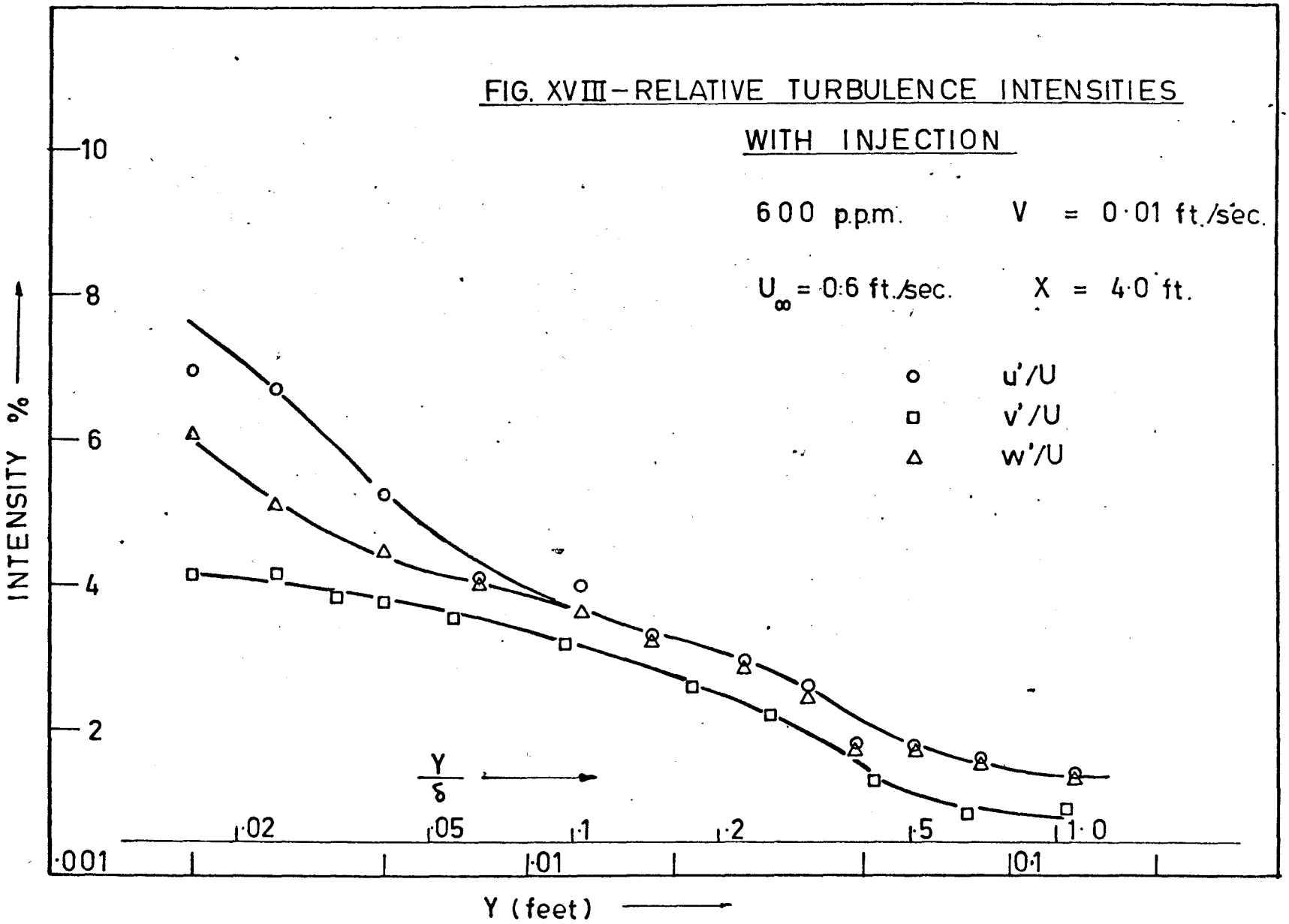
FIG. XVIII – RELATIVE TURBULENCE INTENSITIES
WITH INJECTION
600 p.p.m.
V = 0·01 ft./sec.
U∞ = 0·6 ft./sec.
X = 4·0 ft.
o u'/U
□ v'/U
△ w'/U
INTENSITY %
10
8
6
4
2
Y/δ
·02
·05
·1
·2
·5
1·0
·001
·01
·1
Y (feet)

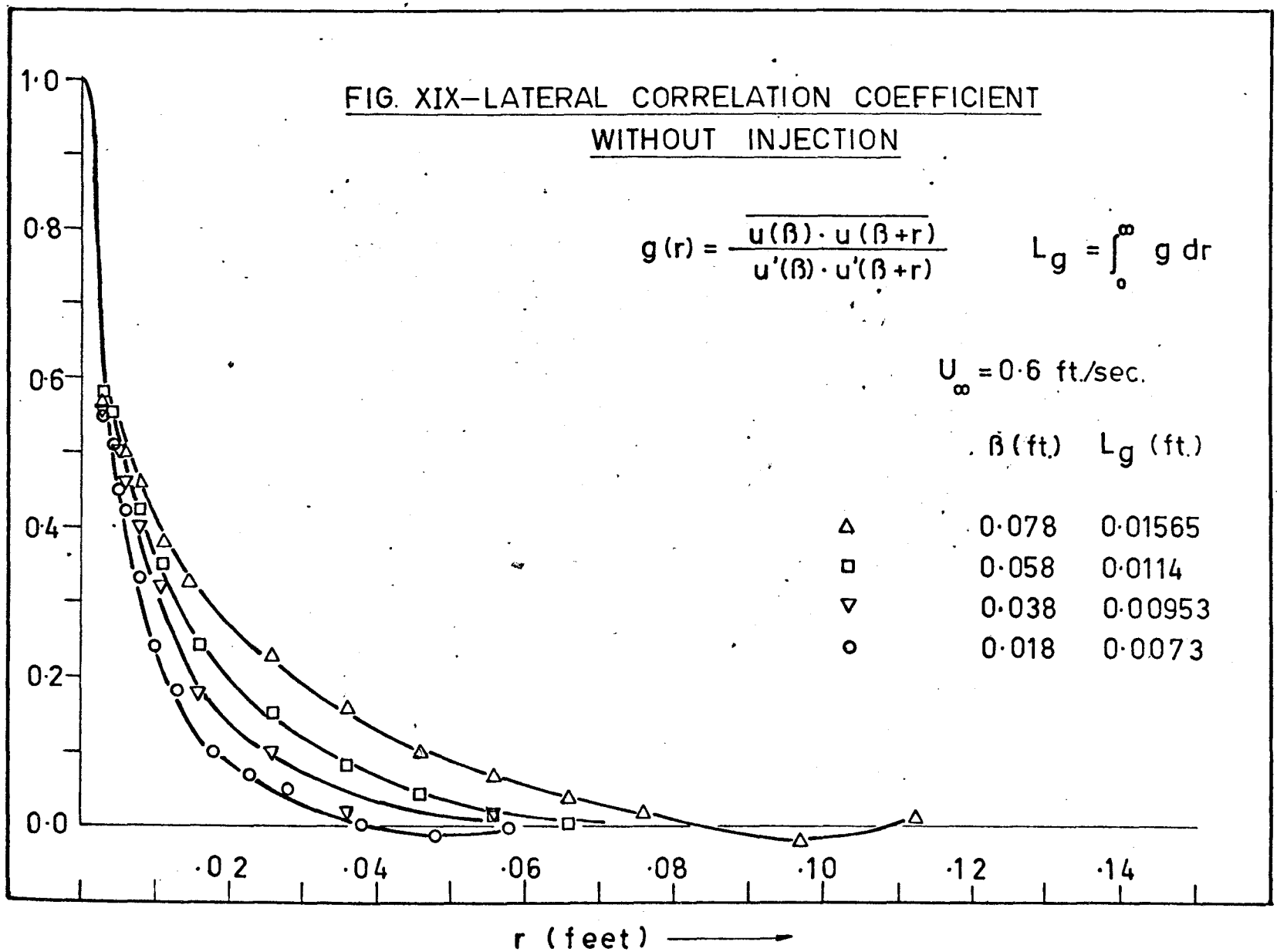
FIG. XIX—LATERAL CORRELATION COEFFICIENT
WITHOUT INJECTION
$g(r) = \frac{\overline{u(\beta) \cdot u(\beta+r)}}{u'(\beta) \cdot u'(\beta+r)}$
$L_g = \int_0^\infty g\, dr$
$U_\infty = 0{\cdot}6$ ft./sec.
ß (ft.) L_g (ft.)
0·078 0·01565
0·058 0·0114
0·038 0·00953
0·018 0·0073
g (r)
1·0
0·8
0·6
0·4
0·2
0·0
·02
·04
·06
·08
·10
·12
·14
r (feet)

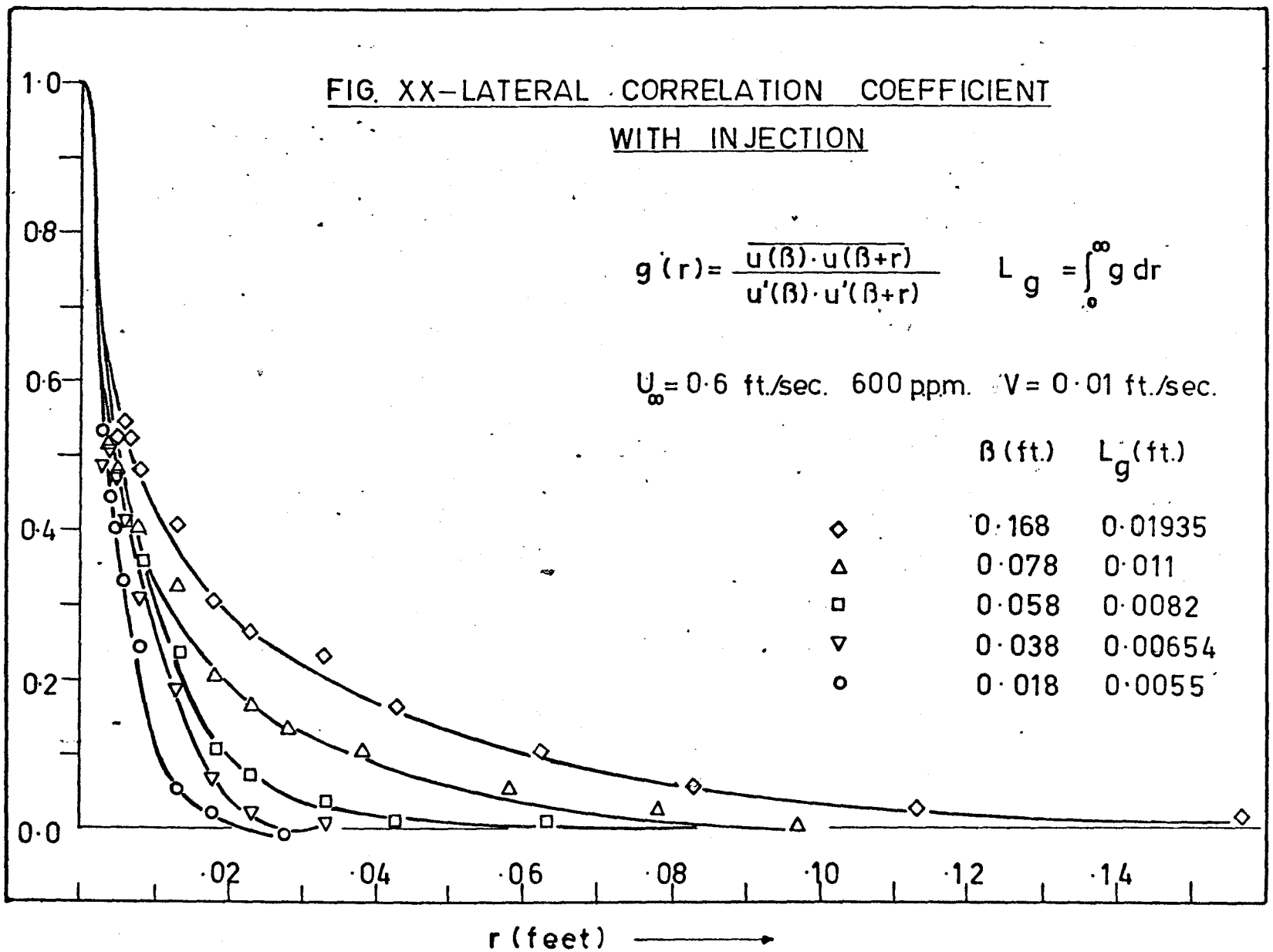
FIG. XX–LATERAL CORRELATION COEFFICIENT
WITH INJECTION
$g(r) = \frac{\overline{u(\beta) \cdot u(\beta+r)}}{u'(\beta) \cdot u'(\beta+r)}$
$L_g = \int_0^\infty g\, dr$
U_∞ = 0·6 ft./sec. 600 ppm. V = 0·01 ft./sec.
β (ft.) L_g (ft.)
◇ 0·168 0·01935
△ 0·078 0·011
□ 0·058 0·0082
▽ 0·038 0·00654
○ 0·018 0·0055
g (r)
1·0
0·8
0·6
0·4
0·2
0·0
·02
·04
·06
·08
·10
·12
·14
r (feet)

FIG. XXI—DISTRIBUTION OF EDDY VISCOSITY

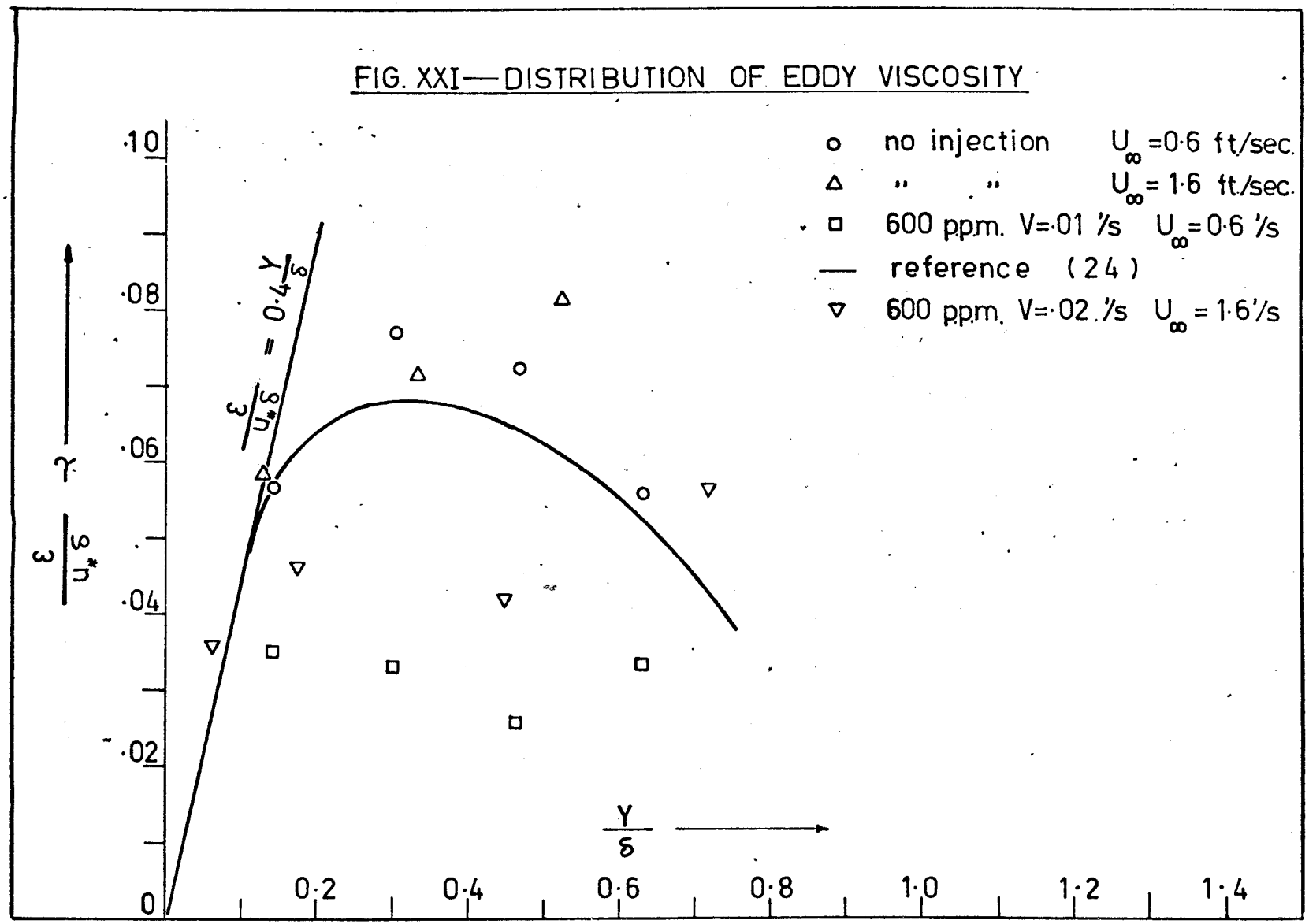

X APPENDIX I

X.1 Estimation of the Drag Reduction by Polymer Solutions:

In the experiment, no direct force measurement had been taken and the drag reduction was estimated in the following manner.

The drag force D on a flat surface of unit width is given by

$$D = \int_0^x \tau_o \, dx \qquad \text{Eq.(X.1)}$$

and

$$D = \rho \int_0^\delta U \, (U_\infty - U) \, dy \qquad \text{Eq.(X.2)}$$

The momentum thickness θ in a boundary layer is defined by

$$\theta \, U_\infty^2 = \int_0^\delta U \, (U_\infty - U) \, dy \qquad \text{Eq.(X.3)}$$

Combining the three equations, we obtain

$$D = \rho \, U_\infty^2 \, \theta \qquad \text{Eq.(X.4)}$$

and

$$\tau_o = \rho \, U_\infty^2 \, \frac{d\theta}{dx} \qquad \text{Eq.(X.5)}$$

With subscript (a) referring to a polymer solution, and assuming no change in free stream velocity U_∞ and liquid density ρ, we have

$$D_a = \rho \, U_\infty^2 \, \theta_a$$

$$\therefore \quad \frac{D - D_a}{D} = \frac{\theta - \theta_a}{\theta} \doteq \frac{\Delta\theta}{\theta}$$

i.e. Percentage drag reduction = $\dfrac{\Delta\theta}{\theta}$ Eq.(X.6)

Owing to the difficulty in assessing the boundary layer thickness from the velocity profiles, the momentum thickness in water, θ , was evaluated from an expression in Schlichting (23), assuming a 1/7th power law velocity profile,

$$\theta = 0{\cdot}036 \times Re_x^{-1/5} \qquad \text{Eq.(X.7)}$$

while $\Delta\theta$ was computed numerically from the two velocity profiles at the same location on the plate surface, viz.,

$$\Delta\theta = \int_0^{\delta} \frac{U}{U_\infty}\left(1 - \frac{U}{U_\infty}\right) dy \; - \left[\int_0^{\delta} \frac{U}{U_\infty}\left(1 - \frac{U}{U_\infty}\right) dy \right]_a$$

For the occurrence of drag reduction,

$$\delta > \delta_a \quad ,$$

and in the interval $\delta \geq y \geq \delta_a$, the expression $\frac{U}{U_\infty}\left(1 - \frac{U}{U_\infty}\right)_a$ is equal to zero. Thus we can change our upper limit of integration of the second integral into δ . Denoting the velocity ratio $\frac{U}{U_\infty}$ by η , then

$$\Delta\theta = \int_0^{\delta} (\eta - \eta^2)\, dy \; - \int_0^{\delta} (\eta_a - \eta_a^2)\, dy$$

$$= \int_0^{\delta} (\eta_a - \eta)(\eta_a + \eta - 1)\, dy$$

$$\therefore \quad \Delta\theta = \Delta y \sum_{i=1}^{n} (\eta_a - \eta)_i (\eta_a + \eta - 1)_i \qquad \text{Eq.(X.8)}$$

The above expression is more suitable in the numerical computation process.

X.2 Estimation of the Local Skin Friction Coefficient of a Polymer Solution:

It is derived in Eq.(X.5) that

$$\tau_o = \rho U_\infty^2 \frac{d\theta}{dx}$$

By the definition of the local skin friction coefficient

$$C_f = \frac{\tau_o}{1/2 \cdot \rho U_\infty^2}$$

Combining these two, we get

$$C_f = 2 \cdot \frac{d\theta}{dx} \qquad \text{Eq.(X.9)}$$

Integrating with respect to x from x_2 to x_1, while θ increases from θ_2 to θ_1, then

$$\int_{\theta_2}^{\theta_1} d\theta = \frac{1}{2} \int_{x_2}^{x_1} C_f \, dx$$

If we assume C_f to remain constant over a small distance $\Delta x = x_1 - x_2$, then

$$\theta_1 - \theta_2 = \frac{1}{2} \Delta x \cdot C_f \qquad \text{Eq.(X.10)}$$

Similarly, for the polymer solution,

$$\theta_{1,a} - \theta_{2,a} = \frac{1}{2} \Delta x_a \cdot C_{f,a} \qquad \text{Eq.(X.11)}$$

In the experiment, it was found that the variation of the local skin friction coefficient was not very large over relatively long distances; hence, choosing the point x_2 where $\theta_{2,a} = \theta_2$, Eq.(X.11) becomes

$$\theta_{1,a} - \theta_2 = \frac{1}{2} \Delta x \cdot C_{f,a} \qquad \text{Eq.(X.12)}$$

Combining equations (X.10) and (X.12) we obtain

$$\frac{C_{f,a}}{C_f} = \frac{\theta_{1,a} - \theta_2}{\theta_1 - \theta_2} = \frac{\theta_{1,a}\left(1 - \frac{\theta_2}{\theta_{1,a}}\right)}{\theta_1\left(1 - \frac{\theta_2}{\theta_1}\right)}$$

Again, for the drag reduction to occur, $\theta_1 > \theta_{1,a}$

i.e. $$\left(1 - \frac{\theta_2}{\theta_1}\right) > \left(1 - \frac{\theta_2}{\theta_{1,a}}\right)$$

$$\therefore \quad \frac{C_{f,a}}{C_f} < \frac{\theta_{1,a}}{\theta_1}$$

In order to see what is the value of $C_{f,a}$, the inequality expression is approximated to an equation. Thus,

$$C_{fa} = C_f \cdot \frac{\theta_{1,a}}{\theta_1} \qquad \text{Eq.(X.13)}$$

The value C_{fa} obtained in this way is bigger than the actual value. This means that the actual curves in Figure XVI should

be shifted still higher; the present plot gives a conservative picture on the apparent thickening of the viscous sublayer.

X.3 Sample Calculations:

Consider the test run having the following data. (Fig.XV).

U_∞ = 1·6 ft/sec.

x = 4 ft.

V = 0.0084 ft/sec

Concentration = 600 p.p.m.

$$\text{Local Reynolds Number} = \frac{U_\infty x}{\nu}$$

$$= \frac{1{\cdot}6 \times 4}{10^{-5}} = 6{\cdot}4 \times 10^5$$

From equation (X.7), the momentum thickness θ in water is

$$\theta = 0.036 \times R_{ex}^{-1/5}$$

$$= 0.036 \times 4 \times (6.4 \times 10^5)^{-1/5} = 0.00994 \text{ ft.}$$

From the velocity profiles and using Eq. (X.8)

$$\Delta\theta = 0.00197 \text{ ft.}$$

Therefore the estimated percentage drag reduction = $\frac{\Delta\theta}{\theta}$

= 19.85%

In reference (23), an expression was given for the local skin friction coefficient whereby

$$c_f = (2 \log R_{ex} - 0.65)^{-2.3} \qquad \text{Eq.(X.14)}$$

Substituting the values, we get

$$c_f = 0.004$$

Also,

$$\theta_a = \theta - \Delta\theta = 0.00797 \text{ ft.}$$

$$\therefore \quad C_{f,a} = C_f \cdot \frac{\theta_a}{\theta} = 0.00321$$

For the polymer solution,

$$U_{*,a} = U_\infty \sqrt{\frac{C_{fa}}{2}} = 0{\cdot}064 \text{ ft./sec.}$$

as compared to that for water, $U_* = 0{\cdot}0715$ ft./sec.

From the velocity profile in figure (XV), when

$y_a = 0.002$ ft, $\eta_a = 0.38$.

$$\therefore \quad U_a^+ = \frac{U_a}{U_{*,a}} = \eta_a \cdot \frac{U_\infty}{U_{*,a}} = 9.5$$

Furthermore, assuming no significant change in the value of the fluid kinematic viscosity,

$$y_a^+ = \frac{y_a \, U_{*a}}{\nu} = 12.8$$

The curves in figure XVI have all been calculated from the above procedures.

XI APPENDIX II

Relations Between the Longitudinal and Lateral Integral Scales

In an isotropic turbulence field, the longitudinal and the lateral double velocity correlation coefficients are connected by the following expression, (Hinze, ref. 24).

$$g = f + \frac{r}{2} \cdot \frac{\partial f}{\partial r}$$

If we multiply both sides by r then,

$$g \cdot r = f \cdot r + \frac{r^2}{2} \cdot \frac{\partial f}{\partial r} = \frac{1}{2} \cdot \frac{\partial (r^2 \cdot f)}{\partial r}$$

or

$$f = \frac{2}{r^2} \int_0^r g \cdot r \, dr \qquad \text{Eq.(XI.1)}$$

By definition, the integral scales are given by

$$L_f = \int_0^\infty f \, dr \qquad \text{Eq.(XI.2)}$$

$$L_g = \int_0^\infty g \, dr \qquad \text{Eq.(XI.3)}$$

Also, when r is very small, g can be approximated in terms of the lateral micro scale λ_g ref.(24)

$$g = 1 - \frac{r^2}{\lambda_g^2} \qquad \text{Eq.(XI.4)}$$

Substituting Eq.(XI.2) with Eq.(XI·1)

$$L_f = \int_0^\infty \left(\frac{2}{\xi^2} \int_0^\xi g \cdot r \, dr \right) d\xi$$

$$= 2 \int_0^\infty \left(\int_0^\xi g \cdot r \, dr \right) d\left(-\frac{1}{\xi}\right)$$

and integrating by parts,

$$L_f = 2 \left\{ \left[-\frac{\int_0^\xi g r \, dr}{\xi} \right]_0^\infty - \int_0^\infty \left(-\frac{1}{\xi}\right)(g\xi)\, d\xi \right\}$$

$$= 2 \left[\lim_{\xi \to 0} \frac{\int_0^\xi g r \, dr}{\xi} - \lim_{\xi \to \infty} \frac{\int_0^\xi g r \, dr}{\xi} + L_g \right]$$

This can be written in a more concise form as

$$L_f = 2 (I + II + L_g)$$

Substituting Eq.(XI.4) into term I, we get

$$\lim_{\xi \to 0} \frac{\int_0^\xi g r \, dr}{\xi} = \lim_{\xi \to 0} \frac{\int_0^\xi \left(r - \frac{r^3}{\lambda^2 g} \right) dr}{\xi}$$

$$= \lim_{\xi \to 0} \frac{\left(\frac{\xi^2}{2} - \frac{\xi^4}{4\lambda^2 g} \right)}{\xi}$$

$$= \lim_{\xi \to 0} \left(\frac{\xi}{2} - \frac{\xi^3}{4\lambda^2 g} \right) = 0$$

In an isotropic turbulence,

$$\int_0^\infty g r \, dr = 0$$

Hence, term II becomes

$$\lim_{\xi \to \infty} \frac{\int_0^\xi g r \, dr}{\xi} = \frac{\int_0^\infty g r \, dr}{\lim_{\xi \to \infty} \xi} = 0$$

Therefore, $L_f = 2 (0 + 0 + L_g)$

i.e. $$L_f = 2 L_g \qquad \text{Eq.(XI.5)}$$

In reference (24), it was shown that the eddy viscosity ε has the following relationship with the integral scale.

$$\varepsilon = v' L_f \qquad \text{Eq.(XI.6)}$$

where v' is the lateral fluctuating velocity component. It is more usual to plot the values in a dimensionless form and this can be achieved by dividing both sides of Eq.(XI.6) by $U_* \delta$ so that

$$\frac{\varepsilon}{U_* \delta} = \frac{v'}{U_*} \cdot \frac{L_f}{\delta} = \left[\frac{v'}{U}\right] \left[\frac{U}{U_\infty}\right] \left[\frac{U_\infty}{U_*}\right] \left[\frac{L_f}{\delta}\right] \qquad \text{Eq.(XI.7)}$$

The values in each bracket are readily obtained and the distribution of the eddy viscosity in the boundary layer is plotted in figure XXI.

XII APPENDIX III

Velocity Distribution in the Tilting Flume

The test plate, which was at a height of about 6" above the bottom of the channel,was situated about 22 feet from the entrance plenum tank. Since it was essential that the velocity in the majority of the cross section of the channel was uniform, the velocity profiles were measured at two sections upstream of the plate. These sections were at 2 and 4 feet from the leading edge of the plate. At each of these cross sections the vertical velocity distributions were measured at the centre line and on either side of this position at 2-1/2" from each of the glass side walls. The table given below gives the velocity profiles obtained at these positions. It can be observed that the profiles were fairly uniform.

U = 1.6 ft/sec. at y/H = 0.38

Depth of water in the channel H = 1.13 feet

	Dist = 4'			Dist = 2'		
$\frac{y}{H}$	L	Centre	R	L	Centre	R
.38	100%	100%	100%	100%	102%	98.4%
.47	100.6	94.9	100	98.6	101.4	97.1
.56	98.6	101.3	96.8	97.2	97.3	96.3
.65	96.8	103.2	96.8	96.4	99.3	103
.74	93.7	100.8	99.4	95.7	95.9	97.8
.83	93.1	101.3	97.4	92.2	96.5	100.8
.86	90.6	105.2	104.4	92.2	98.6	102.2

XIII APPENDIX IV

Polymer Solution Preparation

The physical properties of the polymers were obtained from the suppliers, Stein-Hall Ltd. The method of preparation of the polymer solutions was the same as that used by Smallman (1). The polymer Polyacrylamide MRL - 295, which was in a fine granular form, was hydroscopic and therefore care was taken to ensure that the given sample was not unduly exposed to moisture from the environment. Prior to mixing the polymer was baked several times in a refractory furnace* in order to thoroughly dry it, and weighed+ after each baking. For a selected concentration, the appropriate mass of the polymer needed was weighed out in a crucible. The solution was prepared directly in the measuring tank of 10 Imp. Gall. capacity. Firstly, the tank was filled half-full with distilled water and the pneumatic stirrer was set into motion. The weighed sample was then gently poured into the eye of the vortex formed by the circular motion of the agitator. The residue left in the crucible was washed into the tank by jets of distilled water from a polyethylene wash bottle. More distilled water was then introduced into the tank so that the solution in the tank was finally made up to the 10 gallon mark. The polymer solution was continually stirred whilst in storage.

---

* Precision Scientific Company, U. S. A. Model 14

\+ Mettler Multi-purpose Balance, Type H5; E. Mettler, Zurich, Switzerland.